Anion−Anion Interactions Involving the $[Mo_3Se_{13}]^{2-}$ Cluster. Syntheses and Characterization of $(Me_4N)_2Mo_3Se_{13}$, $K_2Mo_3Se_{12.5}O_{0.5}$, and $K_6Mo_6Se_{27}\cdot 6H_2O$

Ju-Hsiou Liao,[†] Jing Li,[‡,§] and Mercouri G. Kanatzidis*,[†]

Department of Chemistry and the Center for Fundamental Materials Research, Michigan State University, East Lansing, Michigan 48824, and Department of Chemistry, Rutgers University, Camden, New Jersey 08102

Received September 30, 1994[⊗]

The hydrothermal reaction of MoO_3, Na_2Se_2 and Me_4NCl (molar ratio, 1:3:2) at 135 °C for 3 days gave dark red needles of $(Me_4N)_2Mo_3Se_{13}$ (**I**); the reaction of MoO_3 and K_2Se_2 (molar ratio of 1:2 for one month and 1:3−5 for 3 days) at 135 °C gave black needle-like crystals of $K_2Mo_3Se_{12.5}O_{0.5}$ (**II**) and black chunky crystals of $K_6Mo_6Se_{27}\cdot 6H_2O$ (**III**) respectively. The structures were determined by single crystal X-ray diffraction techniques. Compound **I** crystallizes in the trigonal space group $P3_1m$ (No. 157), $Z = 1$, $a = 11.578(1)$ Å, $c = 6.110(2)$ Å, $V = 709.4(3)$ Å^3. $d_{calc} = 3.42$ g/cm^3, $\mu = 177.99$ cm^{-1}. Number of data measured: 992. Number of unique data: 502. Number of data having $I > 3.0\sigma(I)$: 438. Number of variables = 49. $R/R_w = 6.0/7.5\%$. Compound **II** crystallizes in the monoclinic space group Cm (No. 8), $Z = 2$, $a = 11.874(3)$ Å, $b = 16.834(3)$ Å, $c = 5.820(3)$ Å, $\beta = 116.65(2)°$, $V = 1040(1)$ Å^3, $d_{calc} = 4.45$ g/cm^3. $\mu = 246.64$ cm^{-1}. Number of data measured: 997. Number of unique data: 951. Number of data having $I > 3.0\sigma(I)$: 849. Number of variables = 89. $R/R_w = 4.3/5.3\%$. **III** crystallizes in the monoclinic space group $P2_1/n$ (No. 14), $Z = 4$, $a = 10.21(2)$ Å, $b = 17.84(1)$ Å, $c = 27.04(2)$ Å, $\beta = 98.8(1)°$, $V = 4868(21)$ Å^3, $d_{calc} = 4.15$ g/cm^3. $\mu = 219.98$ cm^{-1}. Number of data measured: 8706. Number of unique data: 7920. Number of data having $I > 3.0\sigma(I)$: 3520. Number of variables = 391. The $[Mo_3Se_{13}]^{2-}$ in **I** and $[Mo_3Se_{12.5}O_{0.5}]^{2-}$ in **II** are isostructural with $[Mo_3S_{13}]^{2-}$, while **III** is the cocrystallization of two $K_2Mo_3Se_{13}$ clusters and one K_2Se. The anions of **I** and **II** are the same except that the triply bridging Se site is partially occupied by O atoms in **II**. Solid state IR and UV/vis spectra are reported. The $[Mo_3Se_{13}]^{2-}$ cluster has been found to possess significant affinity for anionic species, and this has been manifested in all currently known compounds containing this trinuclear cluster. The new compounds reported in this paper also exhibit clearly defined anion−anion weakly bonding interactions. Extended Hückel calculations were performed to explain the unusual $[Mo_3Se_{13}]^{2-}\cdot Se^{2-}$ interactions in these compounds. The calculations show that the Se atoms (of the bridging Se_2^{2-}), which form the points of interaction of the cluster with the anionic species, are weakly positively charged.

Introduction

Molybdenum-sulfur chemsitry has been extensively studied in the last two decades. A great motivation has been the industrial application of sulfide-based catalysts for the hydrodesulfurization reaction[1] (HDS) and the importance of the active site of molybdoenzyme[2] in biological systems. To date, a variety of molybdenum polysulfide complexes[3] have been synthesized and structurally characterized. In contrast, little corresponding Mo/Se chemistry has been reported. Recently, we described the first alkali metal molybdenum polyselenide complexes, $K_{12}Mo_{12}Se_{56}$,[4] $K_8Mo_9Se_{40}\cdot H_2O$,[5] and $K_2Mo_3Se_{18}$[5] prepared by hydrothermal techniques. These compounds contain as building block the $[Mo_3Se_7]^{4+}$ cluster core which is arranged in different ways bridged by covalently bonded Se_x^{2-} chains. The $[Mo_3Q_7]^{4+}$ (Q = S, Se) cores have also been observed by Hegetschweiler et al.[6] and Fedin et al.[7-9] where they are chelated by nucleophilic ligands at the Mo sites. On the basis of this previous work, it is apparent that the K_2Se_x/Mo system is much more versatile than the corresponding sulfur system, particularly in water. Furthermore, from a series of polychalcogenide compounds synthesized earlier in nonaqueous solvents by conventional solution methods, we learned that the

[†] Michigan State University.
[‡] Rutgers University, Camden.
[§] ACS−PRF Summer Faculty Fellow 1993.
[⊗] Abstract published in *Advance ACS Abstracts,* April 1, 1995.

(1) (a) Chianelli, R. R.; Pecoraro, T. A.; Halber, T. R.; Pan, W.-H.; Stiefel, E. I. *J. Catal.* **1984**, *86*, 226−230. (b) Pecoraro, T. A.; Chianelli, R. R. *J. Catal.* **1981**, *67*, 430−445. (c) Harris, S.; Chianelli, R. R. *J. Catal.* **1984**, *86*, 400−412.
(2) Burgess, B. K., In *Advances in Nitrogen Fixation Research*; Veeger, C.; Newton, W. D., Eds.; Nijhoff-Junk-Pudoc: Wageningen, The Netherlands, 1983, and references therein.
(3) (a) Coucouvanis, D.; Hadjikyriacou, A. I.; Draganjac, M.; Kanatzidis, M. G.; Ileperuma, O. *Polyhedron* **1986**, *5*, 349−356. (b) Herberhold, M.; Jin, G.-X.; Müller, A.; Penk, M. *Z. Naturforsch.* **1991**, *46b*, 25−34. (c) Coucouvanis, D.; Koo, S.-M. *Inorg. Chem.* **1989**, *28*, 2−5. (d) Coucouvanis, D.; Toupadakis, A.; Koo, S.-M.; Hadjikyriacou, A. I. *Polyhedron*, **1989**, *8*, 1705−1716. (e) Hadjikyriacou, A. I.; Coucouvanis, D. *Inorg. Chem.* **1987**, *26*, 2400−2408. (f) Hadjikyriacou, A. I.; Coucouvanis, D. *Inorg. Chem.* **1989**, *28*, 2169−2177. (g) Draganjac, M.; Simhon, E.; Chan, L. T.; Kanatzidis, M. G.; Baenziger, N. C.; Coucouvanis, D. *Inorg. Chem.* **1982**, *21*, 3321−3332. (h) Clegg, W.; Mohan, N.; Müller, A.; Neumann, A.; Rittner, W.; Sheldrick, G. M. *Inorg. Chem.* **1980**, *19*, 2066−2069. (i) Müller, A. *Polyhedron* **1986**, *5*, 323−340. (j) Müller, A.; Nolte, W.-O.; Krebs, B. *Angew. Chem. Int. Ed. Engl.* **1978**, *17*, 279. (k) Müller, A.; Nolte, W.-O.; Krebs, B. *Inorg. Chem.* **1980**, *19*, 2835−2836. (l) Xin, X. Q.; Morris, N. L.; Jameson, G. B.; Pope, M. T. *Inorg. Chem.* **1985**, *24*, 3482−3485. (m) Müller, A.; Römer, M.; Römer, C.; Reinsch-Vogell, U.; Bögge, H.; Schimanski, U. *Monatsh. Chem.* **1985**, *116*, 711−717.
(4) Liao, J.-H.; Kanatzidis, M. G. *J. Am. Chem. Soc.* **1990**, *112*, 7400−7402.
(5) Liao, J.-H.; Kanatzidis, M. G. *Inorg. Chem.* **1992**, *31*, 431−439.
(6) Meienberger, M. D.; Hegetschweiler, K.; Rüegger, H.; Gramlich, V. *Inorg. Chim. Acta* **1993**, *213*, 157−169.
(7) (a) Fedin, V. P.; Gubin, S. P.; Mishchenko, A. V.; Fedorov, V. Ye. *Koord. Khim.* **1984**, *10*, 901−906. (b) Fedorov, V. Ye.; Mironov, A. V.; Kuz'mina, O. A.; Fedin, V. P. *Russ. J. Inorg. Chem. (Engl. Transl.)* **1986**, *10*, 1429−1431.

0020-1669/95/1334-2658$09.00/0

size of counterions is important to crystallize certain structure types.[10] Therefore, in addition to using alkali metals as counterions, we introduced organic counterions into the hydrothermal technique. Here we report the synthesis and structural and spectroscopic characterization of three new ternary molybdenum polyselenides, $(Me_4N)_2Mo_3Se_{13}$ (**I**), $K_2Mo_3Se_{12.5}O_{0.5}$ (**II**), and $K_6Mo_6Se_{27}{\cdot}6H_2O$ (**III**). Compounds **I** and **III** contain the trinuclear $[Mo_3Se_7]^{4+}$ moiety found in other molybdenum polyselenides. In **II**, half of the triply bridging Se atoms in the $[Mo_3Se_7]^{4+}$ cores are found to be replaced by oxygen atoms based on the crystallographic data. The parent complex $[Mo_3Se_{13}]^{2-}$ complex has been synthesized in discrete form and is reported here for the first time, even though its sulfur analog, $[Mo_3S_{13}]^{2-}$, has been known and extensively studied since the 1970s.[11]

A peculiar property of the trinuclear $[Mo_3Se(Se_2)_3(Se_2)_2(Se_x)]^{2-}$ ($x = 2, 3, 4$) clusters, in all compounds in which it has been observed, is its significant affinity toward negatively charged atoms or fragments. This is surprising in that an anionic cluster is not expected to exhibit attractive interactions toward another anion especially when those interactions are not of the coordinative kind between a metal and a ligand. This phenomenon was first observed in the aggregate cluster of clusters $[Mo_{12}Se_{56}]^{12-}$.[4] It was later found in other related compounds.[5-9] In this paper we address the nature of these interactions using theoretical molecular orbital extended Hückel calculations, and we show that they are in fact disguised Lewis acid–base interactions.

Experimental Section

Reagents. Mo was purchased from Alpha Products Inc. Other reagents were obtained as follows: molybdenum trioxide (MoO_3), 99.95%, Johnson, Matthey Catalog Co., Ward Hill, MA; selenium powder, −100 mesh, 99.5+%; tetramethylammonium chloride (Me_4NCl), 97%, Aldrich Chemical Co., Inc., Milwaukee, WI; cesium metal, 99.98% purity, AESAR, Johnson Matthey, Seabrook, NH; potassium metal, Baker analyzed, J. T. Baker, Inc., Phillipsburg, NJ 08865; sodium metal, analytical reagents, Mallinckrodt Inc., Paris, KY; methanol, anhydrous, reagent grade; ether, anhydrous, reagent grade, E. Merck, Darmstadt, Germany.

Physical Measurements. Far-IR spectra (600−100 cm^{-1}) were recorded as CsI pellets while mid-IR spectra (4000−400 cm^{-1}) were recorded as KBr pellets. Each sample was ground with dry CsI or KBr homogeneously into a fine powder, and a pressure of ~6 tons was applied to the mixture to make a translucent pellet. The spectra were recorded with a Nicolet 740 Fourier transform infrared spectrometer in 4 cm^{-1} resolution.

Quantitative microprobe analysis was performed on a JEOL 35CF scanning electron microscope (SEM) equipped with Tracor Northern TN5500 X-ray microanalysis attachment. Single crystals of each sample were mounted on an aluminum stub which was coated with conducting graphite paint to avoid charge accumulation on the sample surface under the bombardment of the electron beam during measurements. A standardless quantitative (SQ) analysis program was used to analyze the X-ray spectra obtained. The selenium ratio is always underestimated due to an artifact of the program. An empirical correction factor (×1.6) was applied to the Mo/Se compounds to correctly evaluate the selenium content. The analyses reported here are based on the average of more than three independent measurements on several crystals of each compound. Optical diffuse reflectance spectra were measured at room temperature with a Shimadzu UV−3101PC double beam, double monochromated spectrophotometer. The sample was ground into powder and pressed into a thin layer above $BaSO_4$ on a sample holder. $BaSO_4$ powder was used as reference. The absorption spectrum was calculated from the reflectance data by using the Kubelka-Munk function: $\alpha/S = (1 - R)^2/2R$. R is the reflectance, α is the absorption coefficient, and S is the scattering coefficient, which is practically wavelength independent when the particle size is larger than 5 μm.[12]

Synthesis. All preparation and handling was done under a nitrogen atmosphere in a glovebox. K_2Se_2, K_2Se_4, and Na_2Se_2 starting materials were prepared by using a modified procedure described in the literature.[13]

$(Me_4N)_2Mo_3Se_{13}$ (I). A mixture of MoO_3 (0.072 g, 0.50 mmol), Na_2Se_2 (0.306 g, 1.5 mmol) and Me_4NCl (0.109 g, 1.0 mmol) was loaded into a ~5 mL heavy-wall Pyrex tube in which 0.3 mL of degassed water was added. The tube was frozen in liquid nitrogen and sealed under a vacuum of $\sim10^{-3}$ Torr. The sealed ampule was maintained at 135 °C under autogenous pressure for 3 days and then cooled to room temperature. The growth of needlelike crystals was observed under 135 °C. The product was isolated with DMF and water to remove excess Se_x^{2-} and NaCl and dried with acetone and ether. Dark red needlelike crystals were obtained in ~68% yield (based on MoO_3). Semiquantitative elemental analysis performed on SEM/EDS indicated $Mo_{1.0}Se_{3.7}$. Satisfactory elemental analysis was obtained for C, H, and N. A mid-IR spectrum indicated the presence of Me_4N^+. The product was found insoluble in H_2O, DMF, DMSO, and other common solvents; therefore, no solution UV−vis spectrum was measured.

$K_2Mo_3Se_{12.5}O_{0.5}$ (II). A mixture of MoO_3 (0.36 g, 2.5 mmol) and K_2Se_2 (1.18 g, 5.0 mmol) was loaded into a 21-mL autoclave to which 1.5 mL of degassed water was added. The autoclave was maintained at 135 °C under autogenous pressure for ~27 days and then cooled to room temperature. The product was isolated with methanol and dried with ether. Yield: 61% (based on MoO_3). The needlelike crystals are stable in air. They are insoluble in H_2O and DMF and other common organic solvents like DMSO, acetonitrile, ethylenediamine, etc. Semiquantitative elemental analysis performed on SEM/EDS indicated $K_{0.87}Mo_{1.0}Se_{3.8}$.

$K_6Mo_6Se_{27}{\cdot}6H_2O$ (III). The reaction of MoO_3 (0.072 g, 0.50 mmol), K_2Se_2 (0.472 g, 2.0 mmol) and 0.3 mL of H_2O in a ~5 mL heavy-wall Pyrex tube at 135 °C for 3 days afforded black chunky crystals of $K_6Mo_6Se_{27}{\cdot}6H_2O$ (**III**) in ~34% yield (based on MoO_3). The product was isolated with methanol to remove excess Se_x^{2-} and dried with ether. The black crystals degrade slowly in air and are very soluble in DMF and water, forming reddish brown air-sensitive solutions which become cloudy in several minutes. SEM/EDS semiquantitative elemental analysis indicated ~$K_6Mo_6Se_{28}$.

X-ray Crystallography

X-ray diffraction (XRD) powder patterns were used for the purpose of phase characterization and identification. The XRD patterns were recorded with a Phillips XRD-3000 controlled by PDP 11 computer and operating at 40 kV/35mA. Ni-filtered Cu radiation was used. In order to ensure the homogeneity, d-spacings obtained from XRD powder measurements of the products were compared, and found to be identical; with those calculated from using the atomic coordinates

(8) Fedin, V. P.; Sokolov, M. N.; Geras'ko, O. H.; Virovets, A. V.; Podberezskaya, N. V.; Fedorov, V. Ye. *Inorg. Chim. Acta* **1991**, *187*, 81−90.
(9) Fedin, V. P.; Sokolov, M. N.; Geras'ko, O. A.; Virovets, A. V.; Podberezskaya, N. V.; Fedorov, V. Ye. *Inorg. Chim. Acta* **1991**, *187*, 81−90.
(10) (a) Huang, S.-P.; Kanatzidis, M. G. *Coord. Chem. Rev.* **1994**, *130*, 509−621. (b) Kanatzidis, M. G. *Comments Inorg. Chem.* **1990**, *10*, 161−195.
(11) (a) Müller, A.; Wittneben, V.; Krickenmeyer, E.; Bögge, H.; Lemke, M. *Z. Anorg. Allg. Chem.* **1991**, *605*, 175−188. (b) Fedin, V. P.; Kolesov, B. A.; Mironov, Yu. V.; Fedorov, V. Ye. *Polyhedron* **1989**, *8*, 2419−2423. (c) Müller, A.; Jostes, R.; Jaegermann, W.; Bhattacharyya, R. G. *Inorg. Chim. Acta* **1980**, *41*, 259−263. (d) Müller, A.; Bhattacharyya, R. G.; Pfefferkorn, B. *Chem. Ber.* **1979**, *112*, 778−780. (e) Müller, A.; Dartmann, M.; Cohen, J. P.; Bennett, J. M.; Kirchner, R. M. *Z. Naturforsch.* **1979**, *34b*, 434−436. (f) Müller, A.; Sarkar, S.; Bhattacharyya, R. G.; Pohl, S.; Dartmann, M. *Angew. Chem., Int. Ed. Engl.* **1978**, *17*, 535. (g) Fedin, V. P.; Kolesov, B. A.; Mironov, Yu. V.; Fedorov, V. Ye. *Polyhedron* **1989**, *8*, 2419−2423.
(12) (a) Kubelka, P.; Munk, F. *Z. Tech. Phys.* **1931**, *12*, 539. (b) Kubelka, P. *J. Opt. Soc. Am.* **1948**, *38*, 448. (c) Wendlandt, W. W.; Hecht, H. G. *Reflectance Spectroscopy*; Interscience Publishers: New York, 1966. (d) Kotüm, G. *Reflectance Spectroscopy*; Springer Verlag: New York, 1969. (e) Tandon, S. P.; Gupta, J. P. *Phys. Status Solidi* **1970**, *38*, 363−367.
(13) Klemm, W.; Sodomann, H.; Langmesser, P. *Z. Anorg. Allg. Chem.* **1939**, *241*, 281−304.

Table 1. Summary of Crystallographic Data for $(Me_4N)_2Mo_3Se_{13}$, $K_2Mo_3Se_{12.5}O_{0.5}$, and $K_6Mo_6Se_{27}{\cdot}6H_2O$

	I	II	III
formula	$(Me_4N)_2Mo_3Se_{13}$	$K_2Mo_3Se_{12.5}O_{0.5}$	$K_6Mo_6Se_{27}{\cdot}6H_2O$
fw	1462.59	1360.39	3044.20
a, Å	11.578(1)	11.874(3)	10.21(2)
b, Å	11.578(1)	16.834(3)	17.84(1)
c, Å	6.110(2)	5.820(3)	27.04(2)
α, deg	90.0	90.0	90.0
β, deg	120.0	116.65(2)	98.8(3)
γ, deg	90.0	90.0	90.0
Z, V, Å^3	1, 709.4(3)	2, 1040(1)	4, 4868(21)
space group	$P3_1m$ (No. 157)	Cm (No. 8)	$P2_1/n$ (No. 14)
d_{calc}, g/cm^3	3.423	4.448	4.153
radiation[a]	Mo Kα (λ = 0.710 69 Å)	Mo Kα (λ = 0.710 69 Å)	Mo Kα (λ = 0.710 69 Å)
μ(Mo Kα), cm^{-1}	177.96	237.81	219.98
final R/R_w,[b] %	6.0/7.5	4.3/5.3	7.2/9.2
temp, °C	23	−100	−130

[a] $3 < 2\theta < 50°$. [b] $R = \sum||F_o| - |F_c||/\sum|F_o|$; $R_w = \{\sum w(|F_o| - |F_c|)^2/\sum w|F_o|^2\}^{1/2}$.

Table 2. Positional Parameters and Equivalent Isotropic Displacement Values (Å^2)[a] for $(Me_4N)_2Mo_3Se_{13}$ with Estimated Standard Deviations in Parentheses

atom	x	y	z	B (eq)
Mo	0	0.1388(3)	0.5262	1.6(2)
Se(1)	0	0	0.827(1)	2.3(2)
Se(2)	−0.2596(4)	0	0.562(1)	2.3(2)
Se(3)	−0.1719(4)	0	0.2265(9)	2.1(2)
Se(4)	0	0.3585(4)	0.423(1)	3.1(2)
Se(5)	0	0.3057(4)	0.790(1)	2.9(2)
N	1/3	2/3	1.014(8)	3(1)
C(1)	1/3	2/3	0.74(1)	0.1
C(2)	0.208(5)	0.657(5)	1.055(7)	5(1)

[a] $B(eq) = 4/3[a^2\beta_{11} + b^2\beta_{22} + c^2\beta_{33} + ab(\cos\gamma)\beta_{12} + ac(\cos\beta)\beta_{13} + bc(\cos\alpha)\beta_{23}]$.

Table 3. Positional Parameters and Equivalent Isotropic Displacement Values (Å^2)[a] for $K_2Mo_3Se_{12.5}O_{0.5}$ with Estimated Standard Deviations in Parentheses

atom	x	y	z	B(eq)
Mo(1)	1.0000	0	0	0.97(8)
Mo(2)	0.7739(2)	0.0823(1)	−0.2020(4)	0.88(5)
Se(1)	0.8481(6)	0	0.166(1)	2.0(2)
Se(2)	0.5660(3)	0	−0.3392(6)	1.4(1)
Se(3)	0.6606(3)	0	−0.6094(6)	1.1(1)
Se(4)	0.6490(2)	0.2125(1)	−0.4152(5)	1.84(8)
Se(5)	0.6858(2)	0.1837(1)	0.0072(5)	2.02(8)
Se(6)	0.9899(2)	0.1548(1)	0.0431(5)	1.37(7)
Se(7)	0.9419(2)	0.1028(1)	−0.3562(4)	1.10(6)
Se(8)	1.2377(3)	0	0.1057(7)	3.0(1)
Se(9)	1.1886(3)	0	0.4518(6)	1.7(1)
K(1)	0.8500(6)	0.3280(4)	0.460(2)	4.3(3)
0	0.8481	0	0.1665	2.0

[a] $B(eq) = 4/3[a^2\beta_{11} + b^2\beta_{22} + c^2\beta_{33} + ab(\cos\gamma)\beta_{12} + ac(\cos\beta)\beta_{13} + bc(\cos\alpha)\beta_{23}]$.

determined from the single crystal data. The calculation of d-spacings was performed with the POWD 10 program.[14] The comparison tables between the calculated and observed d-spacings for these compounds are given in the supplementary material.

The crystal data for $(Me_4N)_2Mo_3Se_{13}$ (**I**), $K_2Mo_3Se_{12.5}O_{0.5}$ (**II**), and $K_6Mo_6Se_{27}{\cdot}6H_2O$ (**III**) were collected on a Rigaku AFC6S diffractometer with graphite monochromated Mo Kα radiation by using an $\omega-2\theta$ scan mode for **I** and **II** and an ω scan mode for **III**. The crystals of **I**−**III** were mounted on the tip of glass fibers. Accurate unit cell parameters for all compounds were obtained from the least-squares refinement of the 2θ, ω, χ, and ϕ values of 20−25 machine-centered

(14) Smith, D. K.; Nichols, M. C.; Zolensky, M. E. POWD 10: A FORTRAN Program for Calculating X-ray Powder Diffraction Patterns, Version 10. The Pennsylvania State University, 1983.

Table 4. Positional Parameters and Equivalent Isotropic Displacement Values (Å^2)[a] for $K_6Mo_6Se_{27}{\cdot}6H_2O$ with Estimated Standard Deviations in Parentheses

atom	x	y	z	B(eq)
Mo(1)	0.3963(4)	0.2027(3)	0.1598(1)	0.6(2)
Mo(2)	0.5921(4)	0.2652(2)	0.1116(1)	0.6(2)
Mo(3)	0.3746(4)	0.3501(3)	0.1285(1)	0.5(2)
Mo(4)	0.4471(4)	0.2783(2)	0.3877(1)	0.6(2)
Mo(5)	0.6723(4)	0.3551(2)	0.4287(2)	0.7(2)
Mo(6)	0.6888(4)	0.2051(2)	0.4053(2)	0.7(2)
Se(1)	0.3590(5)	0.2417(3)	0.0701(2)	1.0(2)
Se(2)	0.5894(5)	0.1233(3)	0.1321(2)	1.1(2)
Se(3)	0.6385(5)	0.2090(3)	0.1991(2)	1.0(2)
Se(4)	0.5450(5)	0.3987(3)	0.0737(2)	0.9(2)
Se(5)	0.6123(5)	0.3876(3)	0.1611(2)	0.9(2)
Se(6)	0.1841(5)	0.2809(3)	0.1629(2)	1.2(2)
Se(7)	0.3771(5)	0.3112(3)	0.2187(2)	0.8(2)
Se(8)	0.2502(5)	0.0846(3)	0.1411(2)	1.5(2)
Se(9)	0.3325(6)	0.1068(3)	0.2262(2)	1.5(2)
Se(10)	0.6930(5)	0.2315(3)	0.0315(2)	1.3(2)
Se(11)	0.8472(5)	0.2659(3)	0.1023(2)	1.1(2)
Se(12)	0.1955(6)	0.4260(3)	0.0709(2)	1.6(2)
Se(13)	0.2804(6)	0.4819(3)	0.1475(2)	1.7(2)
Se(14)	0.5704(5)	0.2528(3)	0.4735(2)	0.8(2)
Se(15)	0.4359(5)	0.4148(3)	0.4213(2)	0.9(2)
Se(16)	0.5288(5)	0.3937(3)	0.3469(2)	0.9(2)
Se(17)	0.8898(5)	0.2778(3)	0.4525(2)	1.0(2)
Se(18)	0.8201(5)	0.3056(3)	0.3679(2)	0.7(2)
Se(19)	0.4646(5)	0.1336(3)	0.3766(2)	0.7(2)
Se(20)	0.5495(5)	0.2130(3)	0.3198(2)	0.8(2)
Se(21)	0.2109(5)	0.2561(3)	0.4099(2)	1.1(2)
Se(22)	0.2231(5)	0.2878(3)	0.3267(2)	1.3(2)
Se(23)	0.7476(6)	0.4285(3)	0.5103(2)	1.4(2)
Se(24)	0.7879(5)	0.4877(3)	0.4376(2)	1.2(2)
Se(25)	0.7873(5)	0.0876(3)	0.4560(2)	1.1(2)
Se(26)	0.8259(6)	0.0965(3)	0.3715(2)	1.3(2)
Se(27)	0.6584(5)	0.3396(3)	0.2665(2)	1.0(2)
K(1)	0.378(1)	0.5822(8)	0.0518(5)	3.1(3)
K(2)	0.610(1)	−0.0474(7)	0.3999(4)	1.6(2)
K(3)	0.063(2)	0.1357(9)	0.2919(5)	3.7(3)
K(4)	0.955(1)	0.1028(8)	0.0548(5)	2.5(3)
K(5)	0.593(2)	0.076(1)	0.9385(6)	4.1(4)
K(6)	0.626(2)	0.008(1)	0.2429(6)	4.2(4)
O(1)	0.134(4)	0.605(2)	−0.002(1)	2.6(8)
O(2)	0.499(3)	−0.071(2)	0.302(1)	1.3(7)
O(3)	0.887(4)	0.029(2)	0.247(1)	2.3(8)
O(4)	−0.031(4)	0.124(2)	0.177(1)	4(1)
O(5)	−0.050(5)	0.279(3)	0.243(2)	6(1)

[a] $B(eq) = 4/3[a^2\beta_{11} + b^2\beta_{22} + c^2\beta_{33} + ab(\cos\gamma)\beta_{12} + ac(\cos\beta)\beta_{13} + bc(\cos\alpha)\beta_{23}]$.

reflections. The intensities of three check reflections were monitored every 150 reflections to detect possible decay during the data collection period. No significant decay was observed. An empirical absorption correction was applied to all data based on ψ scans for three reflections. An additional absorption correction following the DIFABS[15] procedure was applied to isotropically refined data. The structures of **I**−**III** were solved with direct methods (SHELXS-86)[16] and were refined by full-matrix least-squares techniques with the TEXSAN[17] package of crystallographic programs running on a VAXstation 3100/76 computer. The enantiomorphs of **I** and **II** were checked by refining their $(-x, -y, -z)$ coordinates and no significant improvement of R/R_w values and standard deviations of bond distances and bond angles was observed. During the refinement of the structure of **II**, it was found that the temperature factor of one of the Se atoms (the μ_3-Se) was quite large relative to those for the rest of the Se atoms. This implied to us that perhaps another lighter atom may occupy that site either totally or part of the time. Given the fact that no Cl^- ions were detected by

(15) DIFABS: Walker, N.; Stuart, D. DIFABS: An Empirical Method for Correcting Diffraction Data for Absorption Effects. *Acta Crystallogr.* **1983**, *A39*, 158−166.

(16) Sheldrick, G. M. In *Crystallographic Computing 3*; Sheldrick, G. M.; Kruger, C.; Goddard, R., Eds.; Oxford University Press: Oxford, U.K., 1985; pp 175−189.

(17) TEXSAN-TEXRAY Structure Analysis Package, Molecular Structure Corporation, 1985.

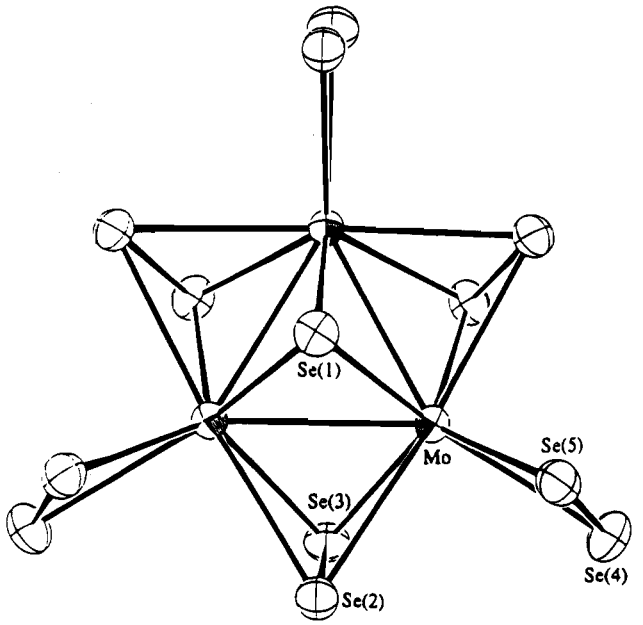

Figure 1. ORTEP representation and labeling scheme of $[Mo_3Se_{13}]^{2-}$.

SEM/EDS analysis in the product, the most probable atom for that site was deemed to be oxygen. Replacement of the μ_3-Se atom with oxygen followed by full-matrix least-squares refinement resulted in a negative temperature factor for that atom. The best results were obtained when a 50:50 ratio of Se and O was used both in terms of achieving a better goodness of fit and R/R_w values and in terms of obtaining a reasonable temperature factor for that site. Of course, the use of this model makes any Mo−Se(O) bond lengths meaningless for comparison purposes. The data collection parameters and details of the structure solution and refinement are given in Table 1. The final atomic coordinates, temperature factors and their estimated standard deviations for **I**−**III** are given in Tables 2−4.

Results and Discussion

Synthesis. The syntheses of **I**−**III** were performed in either thick wall Pyrex-glass tubes or autoclaves at ~135 °C. A very small amount of water is used (~6% filling), and at no time during the reaction is it completely evaporated. The crystals grow in the liquid phase of the container. The small volume of water used is beneficial because it generates supersaturation conditions and promotes crystal growth. The crystals formed during the isotherm of 135 °C and not during the cooldown period. These reactions involve complicated redox chemistry between MoO_3 and Se_2^{2-}. All the structures contain trimeric $[Mo_3(Se_2)_3Q]^{4+}$ (Q = Se for **I** and **III**; Q = $Se_{0.5}O_{0.5}$ for **II** cores as building blocks in which the formal oxidation state of Mo can be assigned as +4. MoO_3 was chosen as a starting material because it possesses the advantage of giving clean reactions by replacing oxygen atoms with Se, forming $[MoSe_xO_{4-x}]^{2-}$ and OH^- in water. The mixed oxoselenometalates $[MoSe_xO_{4-x}]^{2-}$ and $[MQ_4]^{n-}$ (M = Mo, W; Q = S, Se) have been used as starting materials[14] in synthesis at ambient temperature. Subsequent reactions are presumably intramolecular electron transfer or self-redox in nature followed by assembly of metal centers and chelating polychalcogenide ligands. As mentioned earlier when discussing **II**, there exists a mixture of $[Mo_3Se_{13}]^{2-}$ and $[Mo_3Se_{12}O]^{2-}$. This is somewhat surprising, and it is the first time this cluster type is found to contain a μ_3-O ion. Its presence could be rationalized by the very basic nature of the hydrothermal solutions in which the cluster assembles. It is conceivable that under certain conditions, where the concentration of selenide is insufficient and that of OH^- high, the latter could compete effectively in coordinating to Mo. The size of the Se_x^{2-} polyselenide chains

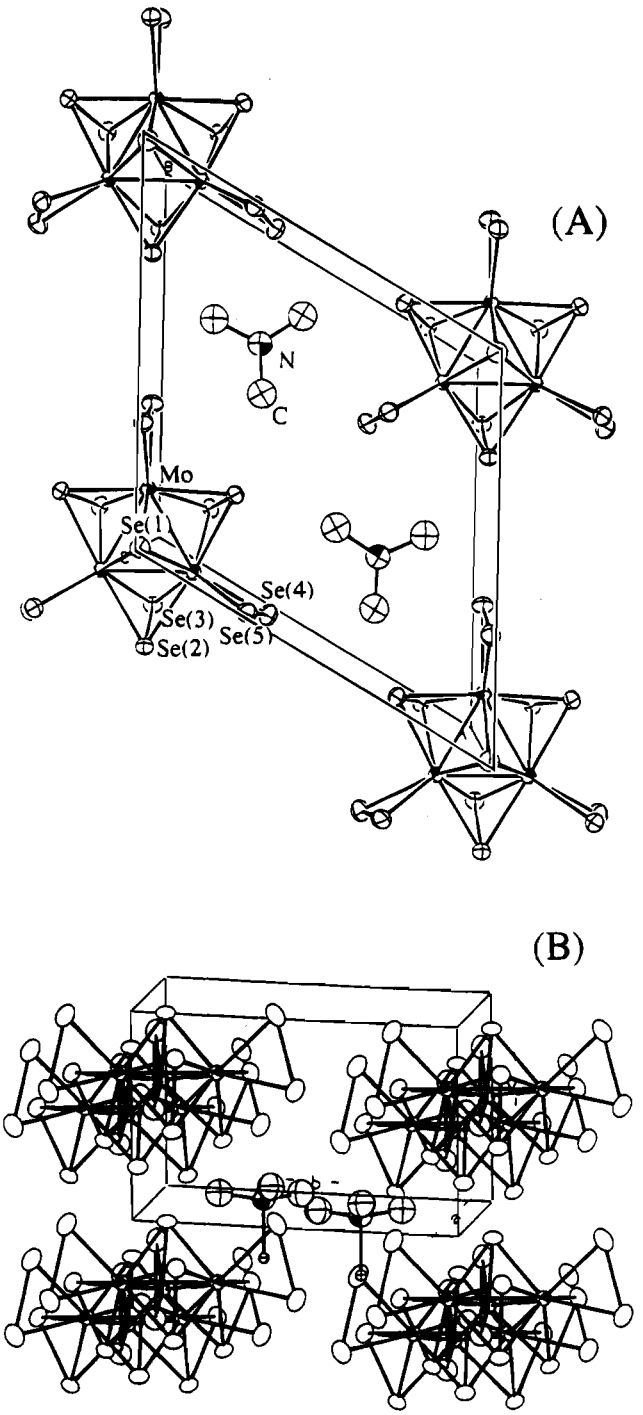

Figure 2. Labeling scheme and packing diagram of $(Me_4N)_2Mo_3Se_{13}$. View down (A) the *c*-axis and (B) the a-axis.

are crucial in these reactions. To avoid the formation of elemental selenium, shorter polyselenide chains have to be used. The Se_2^{2-} was found to be the best polyselenide when MoO_3 is used as the molybdenum source.

The fact that $[Mo_3Se_7]^{4+}$ core occurs in **I**−**III** and in $K_{12}Mo_{12}Se_{56}$,[4] $K_8Mo_9Se_{40}{\cdot}4H_2O$,[5] and $K_2Mo_3Se_{18}$,[5] all of which were made hydrothermally, attests to the core's considerable thermodynamic stability. In solution, the trinuclear $[Mo_3Se_7]^{4+}$ core is probably ligated by Se_x^{2-} ligands. The various $\{[Mo_3Se_7](Se_x)_n\}^{z-}$ complexes present in solution during the reaction provide an efficient mass-transport and dissolution-reprecipitation mechanism, both of which are necessary for crystal growth. Thus the excess Se_x^{2-} ligands act as effective "mineralizers". The role of counterion in phase formation is not clear at the moment but it appears that it too can influence the crystallization outcome.

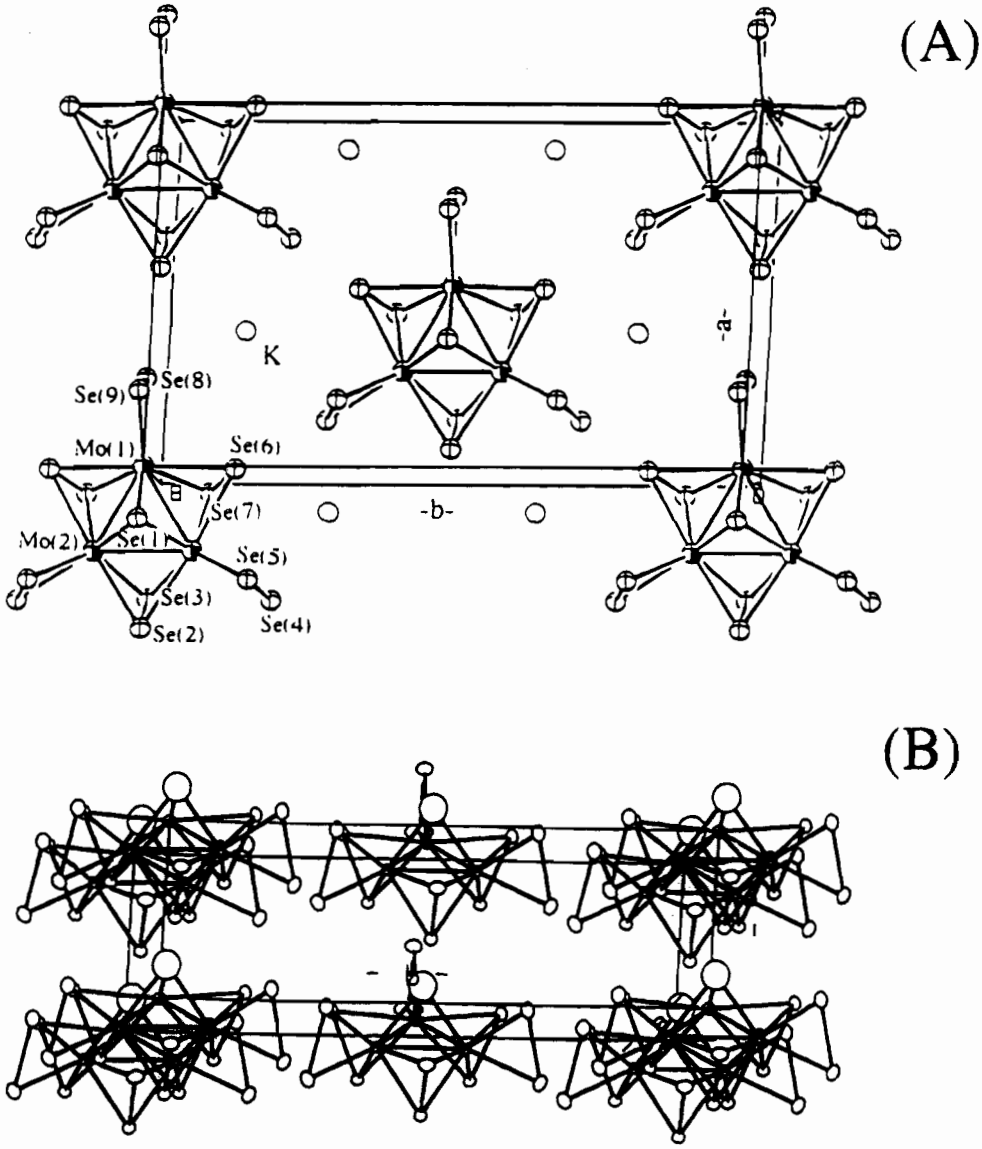

Figure 3. Labeling scheme and packing diagram of $K_2Mo_3Se_{12.5}O_{0.5}$. View down (A) the *c*-axis and (B) *a*-axis.

The reaction of MoO_3 and K_2Se_2 in a 1:2 ratio for 3 days consistently gave crystals of $K_8Mo_9Se_{40}{\cdot}4H_2O$.[5] Surprisingly, the same reaction for a prolonged reaction time afforded $K_2Mo_3Se_{12.5}O_{0.5}$ (**II**). However, the reaction is difficult to control. Sometimes a few very large crystals (up to ~7 mm in length) of $K_8Mo_9Se_{40}{\cdot}4H_2O$ were obtained with a prolonged reaction time. $K_2Mo_3Se_{12.5}O_{0.5}$ is likely to be slightly more insoluble than $K_8Mo_9Se_{40}{\cdot}4H_2O$. Therefore, small fluctuations in reaction conditions may alter the reaction route to the growth of larger crystals of $K_8Mo_9Se_{40}{\cdot}4H_2O$. With the addition of $[Me_4N]^+$, only $[Mo_3Se_{13}]^{2-}$ can be crystallized consistently as $(Me_4N)_2[Mo_3Se_{13}]$ (**I**). Na_2Se_2 was used as starting material to avoid the competition of K/Mo/Se phases.

$K_6Mo_6Se_{27}{\cdot}6H_2O$ (**III**) can be expressed more descriptively as $K_4[Mo_3Se_{13}]_2{\cdot}K_2Se{\cdot}6H_2O$. It is a cocrystallization product of two $[Mo_3Se_{13}]^{2-}$ clusters and one Se_2^{2-} anion and it is related to $K_8Mo_9Se_{40}{\cdot}4H_2O$, which is the cocrystallization product of three $[Mo_3Se_{13}]^{2-}$ clusters and one Se_2^{2-} anion. The tendency of such cocrystallization, rare in Mo/S chemistry, is due to the significant affinity of $[Mo_3Se_{13}]^{2-}$ clusters for Se^{2-} anions and will be discussed in detail later.

It is interesting that known Mo/Se anions such as $[MoSe_4]^{2-}$ and $[MoSe_9]^{2-}$,[18] typically synthesized at ambient temperature with conventional solution methods, were not observed under our hydrothermal conditions nor did we observe any $MoSe_2$ formation. We also did not encounter any Mo/Se Chevrel type phases, such as any of the members of the $A_{n-2}[Mo_{3n}Se_{3n+2}]$ (A = alkali ion) family.[19]

Structures of $(Me_4N)_2Mo_3Se_{13}$ (I) and $K_2Mo_3Se_{12.5}O_{0.5}$ (II). The structures of **I** and **II** contain the same $[Mo_3Se_{13}]^{2-}$ anion which is isostructural with $[Mo_3S_{13}]^{2-}$; see Figure 1. The $[Mo_3Se_{13}]^{2-}$ anion is composed of a Mo_3 triangular core, a triply bridging monoselenide, three doubly bridging diselenides and three terminal diselenides in an overall idealized C_{3v} symmetry. Therefore, the formula can be expressed as $[Mo_3(\mu_3\text{-}Se)(\mu_2\text{-}Se_2)_3(Se_2)_3]^{2-}$. By assigning the charges to Se^{2-} and Se_2^{2-}, the formal oxidation state of Mo atoms is 4+. The three axially disposed Se(3) atoms of the three bridging diselenides lie on the opposite side of the Mo_3 plane relative to the triply bridging monoselenide (Se(1)). The other three equatorial Se(2) atoms are almost coplanar to the Mo_3 plane. Each Mo on the corner of the $[Mo_3Se_7]^{4+}$ core is coordinated by a terminal Se_2^{2-} ligand

(18) (a) Müller, A.; Diemann, E.; Jostes, R.; Bögge, H. *Angew. Chem., Int. Ed. Engl.* **1981**, *20*, 934. (b) Müller, A. *Polyhedron* **1986**, *5*, 323. (c) O'Neal, S. C.; Kolis, J. W. *J. Am. Chem. Soc.* **1988**, *110*, 1971–1973.

(19) (a) Potel, M.; Gougeon, P.; Chevrel, R.; Sergent, M. *Rev. Chim. Miner.* **1984**, *21*, 509–536. (b) Chevrel, R.; Sergent, M. *Topics in Current Physics. Superconductivity in Ternary Compounds*; Fisher, O.; Maple, M. P., Eds.; Springer-Verlag: Berlin, 1982. (c) Gougeon, P.; Potel, M.; Sergent, M. *Acta Crystallogr.* **1989**, *C45*, 182–185.

Table 5. Selected Bond Distances (Å) and Angles (deg) for $(Me_4N)_2Mo_3Se_{13}$ with Standard Deviations in Parentheses

Selected Bond Distances (Å)			
Mo−Mo	2.784(6)	Mo−Se(5)	2.515(6)
Mo−Se(1)	2.444(7)	Se(2)−Se(3)	2.290(6)
Mo−Se(2)	2.614(4)	Se(4)−Se(5)	2.320(7)
Mo−Se(3)	2.589(4)	N(1)−C(1)	1.67(8)
Mo−Se(4)	2.620(6)	N(1)−C(2)	1.42(4)
Selected Bond Angles (deg)			
Mo−Mo−Mo	60.00	Se(3)−Mo−Se(3)	83.5(2)
Mo−Mo−Se(1)	55.3(1)	Se(3)−Mo−Se(4)	93.4(1)
Mo−Mo−Se(2)	57.83(9)	Se(3)−Mo−Se(5)	129.4(1)
Mo−Mo−Se(3)	57.47(8)	Se(4)−Mo−Se(5)	53.7(2)
Se(1)−Mo−Se(2)	84.8(1)	Mo−Se(1)−Mo	69.4(2)
Se(1)−Mo−Se(3)	112.2(1)	Mo−Se(2)−Mo	64.3(2)
Se(1)−Mo−Se(4)	145.0(2)	Mo−Se(3)−Mo	65.1(2)
Se(1)−Mo−Se(5)	91.3(2)	Mo−Se(2)−Se(3)	63.3(1)
Se(2)−Mo−Se(2)	169.3(3)	Mo−Se(3)−Se(2)	64.5(1)
Se(2)−Mo−Se(3)	52.2(1)	Mo−Se(4)−Se(5)	60.8(2)
Se(2)−Mo−Se(3)	135.5(2)	Mo−Se(5)−Se(4)	65.5(2)
Se(2)−Mo−Se(4)	93.38(9)	C(1)−N−C(2)	100(3)
Se(2)−Mo−Se(5)	88.7(1)	C(2)−N−C(2)	117(2)

in a side-on fashion. The three terminal diselenides can also be divided into three axial Se atoms (Se(4)) located 1.61 Å below the Mo_3 plane and three equatorial Se atoms (Se(5)) 0.62 Å above the Mo_3 plane. The $[Mo_3Se_7]^{4+}$ core also has been observed in $Mo_3Se_7X_4$ (X = Cl, Br)[7] and $Mo_3Se_7(Et_2NCS_2)_4$.[8] The anionic structure of **II** is the same as that of **I** except that the Mo triply bridging Se atoms are half-occupied by oxygen atoms.

Compound **I** crystallizes in a trigonal space group. As shown in the packing diagram of Figure 2, all the diselenides are sitting in a crystallographic mirror plane. The charge compensating tetramethylammonium cations are sitting in 3 fold rotation axes. Compound **II** is isomorphous to $(NH_4)_2Mo_3S_{13}$.[11] The packing diagram of **II** is shown in Figure 3. The lattice of **II** has lower symmetry than that of **I** because by replacing tetramethylammonium with smaller K^+ cations, the lattice has to be squeezed to achieve a more efficient packing. This results in a shift of the K^+ cations toward the $[Mo_3Se_{12.5}O_{0.5}]^{2-}$ anion and loss of the 3-fold rotation axes.

Selected bond distances and bond angles of **I** and **II** are given in Tables 5 and 6 respectively. The average Mo−Mo distances for **I** and **II** are normal at 2.784(6) and 2.771(1) Å, respectively. The average Mo−Se(1) distance is 2.444(7) Å in **I** and is comparable to those in other $[Mo_3Se_7]^{4+}$-containing compounds.[4,5,7,8] The Mo−Se(3) distances in **I** and Mo−Se(3) and Mo−Se(7) distances in **II** are shorter than those associated with the equatorial Se atoms i.e. Mo−Se(2) in **I** and Mo−Se(2) and Mo−Se(6) in **II**. The former average 2.589(4) and 2.549(3) Å; the latter average 2.614(4) and 2.620(7) Å for **I** and **II**, respectively. The average bridging diselenide Se−Se distances are 2.290(6) and 2.304(2) Å for **I** and **II**; the average Se−Se distance in the terminal diselenides are slightly longer at 2.320(7) and 2.342(6) Å for **I** and **II**, respectively. These values are between the Se−Se distance (2.37 Å) of elemental selenium and that of the Se_2 molecule in the gas phase (2.19 Å).[20]

In the solid state the $[Mo_3(Se_2)_6Q]^{2-}$ anions in **I** and **II** form columnar stacks via short intercluster Se···Se contacts. The triply bridging Se(1) atom of one cluster anion interacts with the three axial selenium atoms of the three bridging diselenides of another below it, as shown in Figure 4. Both Se···Se contacts are significantly shorter than the sum of the van der Waals radius of Se atoms. The short Se···Se contacts vary from 3.147(7) in **I** to 3.034(9) Å in **II**. The difference is likely due to the

(20) Wells, A. F. *Structural Inorganic Chemistry*. Oxford University Press, Oxford, U.K., 1986.

Table 6. Selected Bond Distances (Å) and Angles (deg) for $K_2Mo_3Se_{12.5}O_{0.5}$ with Standard Deviations in Parentheses

Selected Bond Distances (Å)			
Mo(1)−Mo(2)	2.771(2)	Mo(2)−Se(7)	2.552(4)
Mo(2)−Mo(2)	2.772(3)	Se(1)−Se(3)	3.044(9)
Mo(1)−Se(1)(−O)	2.400(8)[a]	Se(1)−Se(7)	3.029(6)
Mo(1)−Se(6)	2.625(2)	Se(2)−Se(3)	2.306(6)
Mo(1)−Se(7)	2.546(2)	Se(4)−Se(5)	2.346(4)
Mo(1)−Se(8)	2.605(4)	Se(6)−Se(7)	2.303(4)
Mo(1)−Se(9)	2.578(3)	Se(8)−Se(9)	2.335(7)
Mo(2)−Se(1) (−O)	2.367(6)[a]	Se(2)−K(1)	3.694(7) × 2
Mo(2)−Se(2)	2.623(4)	Se(4)−K(1)	3.359(8)
Mo(2)−Se(3)	2.548(3)	Se(4)−K(1)	3.400(9)
Mo(2)−Se(4)	2.625(3)	Se(5)−K(1)	3.469(8)
Mo(2)−Se(5)	2.574(4)	Se(8)−K(1)	3.457(8) × 2
Mo(2)−Se(6)	2.612(3)	Se(9)−K(1)	3.461(8) × 2
Selected Bond Angles (deg)			
Mo(2)−Mo(1)−Mo(2)	60.01(8)	Se(1)−Mo(2)−Se(5)	91.4(2)
Mo(1)−Mo(2)−Mo(2)	59.99(4)	Se(1)−Mo(2)−Se(6)	84.4(1)
Mo(2)−Mo(1)−Se(1)	53.9(1)	Se(1)−Mo(2)−Se(7)	111.4(2)
Mo(2)−Mo(1)−Se(6)	57.81(6)	Se(2)−Mo(2)−Se(3)	52.9(1)
Mo(2)−Mo(1)−Se(7)	57.16(8)	Se(2)−Mo(2)−Se(4)	92.41(9)
Mo(2)−Mo(1)−Se(1)	53.9(1)	Se(2)−Mo(2)−Se(5)	88.2(1)
Mo(2)−Mo(1)−Se(6)	57.81(6)	Se(2)−Mo(2)−Se(6)	166.5(1)
Mo(2)−Mo(1)−Se(7)	57.16(8)	Se(2)−Mo(2)−Se(7)	137.9(1)
Se(1)−Mo(1)−Se(6)	83.50(7)	Se(3)−Mo(2)−Se(4)	93.65(9)
Se(1)−Mo(1)−Se(6)	83.50(7)	Se(3)−Mo(2)−Se(5)	130.1(1)
Se(1)−Mo(1)−Se(7)	110.5(1)	Se(3)−Mo(2)−Se(6)	137.9(2)
Se(1)−Mo(1)−Se(7)	110.5(1)	Se(3)−Mo(2)−Se(7)	85.2(1)
Se(1)−Mo(1)−Se(8)	146.7(2)	Se(4)−Mo(2)−Se(5)	53.6(1)
Se(1)−Mo(1)−Se(9)	93.1(2)	Se(4)−Mo(2)−Se(6)	94.40(9)
Se(6)−Mo(1)−Se(6)	165.9(1)	Se(4)−Mo(2)−Se(7)	95.0(1)
Se(6)−Mo(1)−Se(7)	52.85(8)	Se(5)−Mo(2)−Se(6)	86.6(1)
Se(6)−Mo(1)−Se(7)	138.15(7)	Se(5)−Mo(2)−Se(7)	128.6(1)
Se(6)−Mo(1)−Se(8)	93.92(6)	Se(6)−Mo(2)−Se(7)	53.0(1)
Se(6)−Mo(1)−Se(9)	87.62(5)	Mo(1)−Se(1)−Mo(2)	71.1(2)
Se(6)−Mo(1)−Se(7)	138.15(7)	Mo(1)−Se(1)−Mo(2)	71.1(2)
Se(6)−Mo(1)−Se(7)	52.85(8)	Mo(2)−Se(1)−Mo(2)	71.7(2)
Se(6)−Mo(1)−Se(8)	93.92(6)	Mo(2)−Se(2)−Mo(2)	63.8(1)
Se(6)−Mo(1)−Se(9)	87.62(5)	Mo(2)−Se(2)−Se(3)	61.8(1)
Se(7)−Mo(1)−Se(7)	85.6(1)	Mo(2)−Se(2)−Se(3)	61.8(1)
Se(7)−Mo(1)−Se(8)	93.52(9)	Mo(2)−Se(3)−Mo(2)	65.9(1)
Se(7)−Mo(1)−Se(9)	128.64(7)	Mo(2)−Se(3)−Se(2)	65.2(1)
Se(7)−Mo91)−Se(8)	93.52(9)	Mo(2)−Se(3)−Se(2)	65.2(1)
Se(7)−Mo(1)−Se(9)	128.64(7)	Mo(2)−Se(4)−Se(5)	62.1(1)
Se(8)−Mo(1)−Se(9)	53.5(1)	Mo(2)−Se(5)−Se(4)	64.3(1)
Mo(1)−Mo(2)−Se(1)	55.0(2)	Mo(1)−Se(6)−Mo(2)	63.90(7)
Mo(1)−Mo(2)−Se(6)	58.29(7)	Mo(1)−Se(6)−Se(7)	61.82(8)
Mo(1)−Mo(2)−Se(7)	56.98(7)	Mo(2)−Se(6)−Se(7)	62.2(1)
Mo(2)−Mo(2)−Se(1)	54.2(1)	Mo(1)−Se(7)−Mo(2)	65.86(8)
Mo(2)−Mo(2)−Se(2)	58.11(6)	Mo(1)−Se(7)−Se(6)	65.33(9)
Mo(2)−Mo(2)−Se(3)	57.04(5)	Mo(2)−Se(7)−Se(6)	64.9(1)
Se(1)−Mo(2)−Se(2)	83.3(2)	Mo(1)−Se(8)−Se(9)	62.6(1)
Se(1)−Mo(2)−Se(3)	110.6(1)	Mo(1)−Se(9)−Se(8)	63.8(1)
Se(1)−Mo(2)−Se(4)	145.0(2)		

[a] Average between a Mo−Se and a Mo−O distance.

countercations. The potassium ion is smaller than tetramethylammonium so that the $[Mo_3Se_{12.5}O_{0.5}]^{2-}$ are forced to pack more closely in **II** and perhaps as a result half Se(1) atoms are replaced by smaller oxygen atoms. In $(NH_4)_2Mo_3S_{13}$ the corresponding distance of the S···S short contacts is 3.026 Å. Since the size of sulfur atoms is smaller than that of selenium, this interaction, though present, is not as profound as in the selenium system.

Structure of $K_6Mo_6Se_{27}\cdot 6H_2O$ (III). The structure of **III** contains two $[Mo_3Se_{13}]^{2-}$ anions attached to a monoselenide, as shown in Figure 5. The two $[Mo_3Se_{13}]^{2-}$ anions are interacting with a Se^{2-} anion via the six axial Se atoms of the doubly bridging diselenides in the two $[Mo_3Se_{13}]^{2-}$ clusters in a sandwich fashion. This type of $Se^{2-}/[Mo_3Se_{13}]^{2-}$ association was also observed in the structure of $K_8Mo_9Se_{40}\cdot 4H_2O$.[5] In response to the $Se^{2-}/[Mo_3Se_{13}]^{2-}$ short contacts, a marked

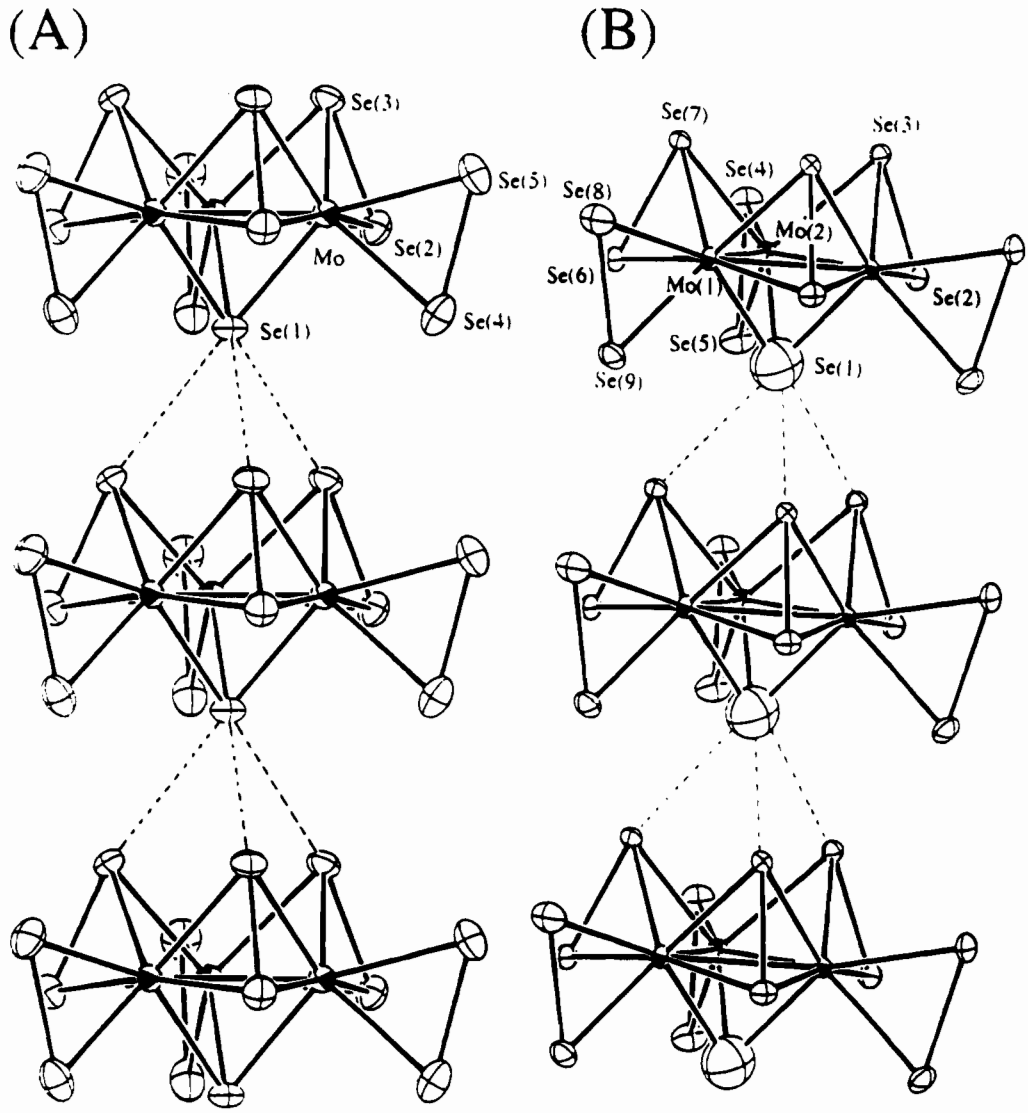

Figure 4. Columnar stacks in (A) $(Me_4N)_2Mo_3Se_{13}$ and (B) $K_2Mo_3Se_{12.5}O_{0.5}$. Dashed lines illustrated Se···Se contacts between the clusters.

lengthening of the Se–Se bonds of the bridging Se_2^{2-} is observed in **III**.

Selected bond distances and bond angles of **III** are given in Table 7. The average Mo–Mo distance is 2.77(1) Å. For both bridging and terminal diselenides, the average Mo–(equatorial Se) distance is also longer than the average Mo–(axial Se) distance (2.61(2) and 2.54 Å for bridging diselenides; 2.63(1) and 2.61(2) Å for terminal diselenides). The average distance from the Mo atom to the triply bridging selenides (Se(1) and Se(14)) is 2.495(9) Å and falls in the range of those for other $[Mo_3Se_7]^{4+}$-containing compounds. Notice that the average Se–Se bridging diselenide distance of 2.36(2) Å is significantly longer than those in **I** and **II**, while the average terminal diselenide distance (2.34(2) Å) remains approximately the same. This Se–Se bond elongation coincides with the fact thtat the Se···Se contacts between Se^{2-} and $[Mo_3Se_{13}]^{2-}$ are shorter than those observed in **I** and **II**. The Se···Se short contacts between Se(27) and the six axial selenium atoms of the bridging diselenides in the two $[Mo_3Se_{13}]^{2-}$ clusters range from 2.81(1) to 3.035(9) Å. As observed earlier, it is again the Se···Se short contacts that cause the lengthening of the bridging diselenides. A similar interaction was found in $[Mo_3(S_2)_3S(dtc)_3]_2S$,[6] (dtc$^-$ = diethyldithiocarbamate), where an extra S^{2-} anion interacts with two $[Mo_3(S_2)_3S]^{4+}$ cores via the six axial S atoms of the six bridging disulfides. The $[Mo_3(S_2)_3S(dtc)_3]_2S$ cluster also adopts a bent geometry as shown in Figure 5 and the bridging disulfides also exhibit significant bond elongation (2.11 Å). In the Mo/S system several examples of anion–$[Mo_3S_7]^{4+}$-core interactions have already been found.[21]

Spectroscopy. The IR spectrum of **I** shows characteristic peaks of tetramethylammonium in the mid-IR region. In the far-IR region, peaks at 451, 370, 333, 308, 279, and 165 cm^{-1} were observed for **I**, and peaks at 439, 364, 334, 312, 297, 210, 165 cm^{-1} were observed for **II**. We assign the peaks at 451 (**I**) and 439 cm^{-1} (**II**) as the vibration of the $(Mo_3-\mu_3\text{-Se})$ moiety by comparing it to the IR-spectrum of $(NH_4)_2Mo_3S_{13}$, in which the $(Mo_3-\mu_3\text{-S})$ vibration is assigned at 459 cm^{-1}. The peak at 165 cm^{-1} (**I** and **II**) can be assigned as a Mo–Mo vibration. The peaks between 210 and 370 cm^{-1} can be assigned as Mo–Se or Se–Se vibrations. Compound (**III**) did not give any clearly defined peaks in the far-IR region.

The UV-Visible spectra of $K_6Mo_6Se_{27}{\cdot}6H_2O$ were taken in DMF and DMSO. Both solutions, prepared in a N_2 glovebox, gave reddish brown colors and gave two broad bands at around 405 and 480 nm. The $(Me_4N)_2Mo_3Se_{13}$ is sparingly soluble in DMF and a good solution spectrum could not be obtained. Its solid state optical spectrum, however, is shown in Figure 6.

(21) (a) Zimmermann, H.; Hegetschweiler, K.; Keller, T.; Gramlich, V.; Schmalle, H. W.; Petter, W.; Schneider, W. *Inorg. Chem.* **1991**, *30*, 4336–4341. (b) Hegetschweiler, K.; Keller, T.; Bäumle, M.; Rihs, G.; Schneider, W. *Inorg. Chem.* **1991**, *30*, 4342–4347. (c) Fedin, V. P.; Müller, A.; Filipek, K.; Rohlfing, R.; Bögge, H.; Virovets, A. V.; Dziegielewski, J. O. *Inorg. Chim. Acta* **1994**, *223*, 5–7. (d) Klingelhofer, P.; Müller, U.; Friebel, C.; Pebler, J. *Z. Anorg. Allg. Chem.* **1986**, *543*, 22–30.

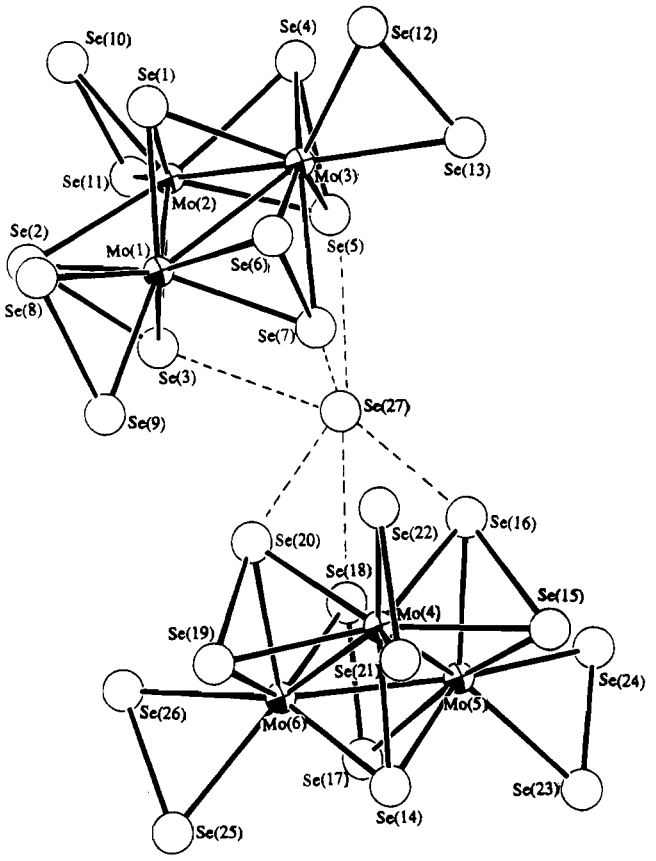

Figure 5. ORTEP representation and labeling scheme of $[Mo_6Se_{27}]^{6-}$. Dashed lines represent Se···Se short contacts.

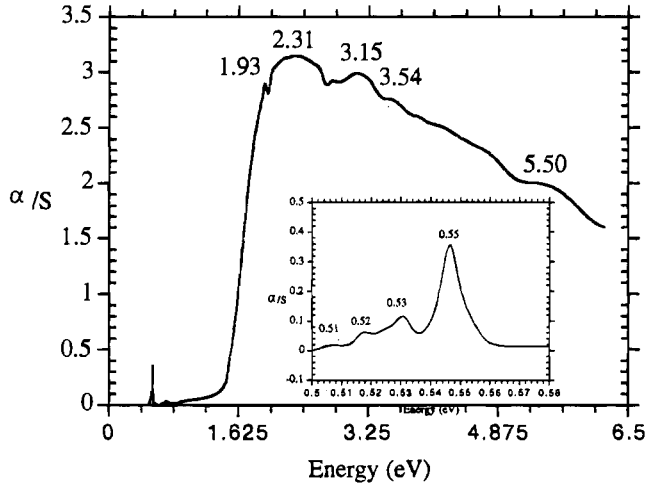

Figure 6. Solid state optical absorption spectrum of $(Me_4N)_2Mo_3Se_{13}$.

The peaks between 0.50 and 0.56 eV are characteristic absorptions of Me_4N^+. $(Me_4N)_2Mo_3Se_{13}$ gives absorption bands above 1.6 eV (775 nm) at 1.93 (642 nm), 2.31 (537 nm), 3.15 (394 nm), 3.54 (350 nm) and 5.50 eV (225 nm). Given that the Mo-trimers are stacked in columns and interact in a head to tail fashion, as described above, it is reasonable to view this material as a quasi-solid-state compound with an extended one-dimensional structure which develops marked electronic band dispersion in the *c*-direction. In this context the material is a semiconductor with bad-gap of 1.6 eV.

Electron Affinity of $[Mo_3Se(Se_2)_3]^{4+}$ Core and the Nature of the Se^{2-}···$[Mo_3Se_{13}]^{2-}$ Interactions. A Molecular Orbital Study. As pointed earlier, the unusual phenomenon observed in all of these molybdenum polyselenide compounds is the tendency of the $[Mo_3Se_7]^{4+}$ cluster to bind, via Se···Se interactions, negatively charged species such as Se^{2-} and Se_x^{2-}. At first glance this seems counterintuitive since negatively charged metal clusters are expected to bind or interact with positive cations. There is a striking inverse correlation between the $Se_{ap}-Se_a$ and the Se_a-Se_b distances, where Se_a and Se_b form the doubly bridging diselenide Se_2^{2-} in the $[Mo_3(\mu_3\text{-Se})(\mu_2\text{-Se}_2)_3]^{4+}$ core, and Se_{ap} can be a triply bridging selenium from another $[Mo_3Se_{13}]^{2-}$ anion, or it can be an isolated Se^{2-} or the terminal Se atom of a Se_x^{2-} ligand. This inverse correlation is clearly demonstrated in Figure 7 which plots Se_a-Se_b distances as a function of $Se_{ap}-Se_a$ distance for all currently known $[Mo_3Se_{13}]^{2-}/Se^{2-}$ interactions (data from six compounds). Table 8 summarizes this information and depicts the common labeling scheme and structural motif used for the purposes of this discussion.

To understand the nature of the $[Mo_3Se_7]^{4+}$···Se interaction we performed a molecular orbital study employing the extended Hückel method.[22] The atomic parameters and a detailed description of the computations are given in ref 23.

Theoretical investigations on the electronic structures of trinuclear early transition metal clusters have been carried out on several molecular systems, including $[Mo_3S_{13}]^{2-}$,[24-26] $[M_3(\mu_3\text{-X})(\mu_2\text{-Y})_3L_9]^{4+}$ (M = Ti, Nb, Mo, W),[24] and $[M_3(\mu_3\text{-X})_2(\mu_2\text{-O}_2\text{Y})_6L_3]$ (M = Mo, W).[23] The important bonding features in these trinuclear clusters have been discussed in much detail and are in accordance with our calculation results on the $[Mo_3Se_{13}]^{2-}$ cluster. Therefore, our focus in the following discussion will be mainly on the systems in which an additional ligand, such as a Se^{2-} anion, is added to the $[Mo_3Se_{13}]^{2-}$ cluster. The bonding interactions between the cluster and the ligand, and the consequence of such interactions will be analyzed.

The model system that we have used in most of our computations consists of a $[Mo_3Se_{13}]^{2-}$ trinuclear cluster and a Se^{2-} anion labeled as $Se(17)^{2-}$. The geometry of $[Mo_3Se_{13}]^{2-}$ is taken from the atomic coordinates of $(Me_4N)_2Mo_3Se_{13}$. The Se^{2-} approaches the trinuclear cluster from the opposite site of the μ_3-Se, as shown in Figure 8. The interatomic distance between Se(8) and $Se(17)^{2-}$ (or between Se(10) and $Se(17)^{2-}$, noting that Se(10) is equivalent to Se(8) by symmetry) was chosen to be slightly different from that between Se(9) and Se^{2-}, as was found in the crystal structure.

Changes in bond strength for various Se_{ap}-Se_a distances are plotted in Figure 9 as the difference in the overlap population[27] $\Delta(O) = OP(d) - OP(\infty)$, where $OP(d)$ is the overlap population at d (Å), a perpendicular distance between Se(17) and the Mo_3

(22) (a) Hoffmann, R. *J. Chem. Phys.* **1963**, *39*, 1397. (b) Hoffmann, R.; Lipscomb, W. N. *J. Chem. Phys.* **1962**, *36*, 2179, 3489; **1962**, *37*, 2872. (c) Ammeter, J. H.; Burgi, H.-B.; Thiebeault, J. C.; Hoffmann, R. *J. Am. Chem. Soc.* **1978**, *100*, 3686.
(23) The atomic parameters for the Mo and Se atoms were taken from ref 28 and 29. The H_{ii}'s (eV) are −9.66 (5s), −6.36 (5p), and −12.30 (4d) for Mo and are −20.50 (4s) and −14.4 (4p) for Se. The exponents and coefficients for double-ζ functions were 1.96 (5s), 1.90 (5p), 4.54, 0.5899 (4d), 1.90, and 0.5899 (4d) for Mo, and are 2.44 (4s) and 2.07 (4p) for Se. The $[Mo_3Se_{13}]^{2-}$ was oriented in such a way that its Mo_3 plane was coincident with the *xy* plane of the Cartesian coordinate system, and its 3-fold rotation axis was parallel to the *z*-axis. The interacting Se^{2-} ion was placed at a perpendicular distance, *d*, from the Mo_3 plane. Calculations on the model system $[Mo_3Se_{14}]^{4-}$ were carried out at d = 3.4, 3.6, 3.8, 4.0, 4.2, and 4.4 Å, which correspond to an Se(8)−Se(17) interatomic distance of 2.466, 2.598, 2.738, 2.885, 3.038, and 3.197 Å, and Se(9)−Se(17) distances of 2.690, 2.811, 2.941, 3.223, and 3.372 Å, respectively.
(24) Müller, A.; Jostes, R.; Cotton, F. A. *Angew. Chem., Int. Ed. Engl.* **1980**, *19*, 875.
(25) Müller, A.; Jostes, R.; Jaegermann, W.; Bhattacharyya, R. G. *Inorg. Chim. Acta* **1980**, *41*, 259.
(26) Müller, A.; Wittneben, V.; Krickemeyer, E.; Bögge, H.; Lemke, M. *Z. Anorg. Allg. Chem.* **1991**, *605*, 175.
(27) Mulliken, R. S. *J. Chem. Phys.* **1955**, *23*, 1833, 1841, 2338, 2343.
(28) Summerville, R. H.; Hoffmann, R. *J. Am. Chem. Soc.* **1979**, *101*, 3821.
(29) Hoffmann, R.; Shaik, S.; Scott, J. C.; Whangbo, M.-H.; Foshee, M. J. *J. Solid State Chem.* **1980**, *34*, 263.

Table 7. Selected Bond Distances (Å) and Angles (deg) for $K_6Mo_6Se_{27}\cdot 6H_2O$ with Standard Deviations in Parentheses

Selected Bond Distances (Å)

Mo(1)−Mo(2)	2.781(9)	Se(17)−Se(18)	2.341(8)	Mo(4)−Se(15)	2.607(7)	Se(15)−K(4)	3.56(1)
Mo(1)−Mo(3)	2.761(7)	Se(19)−Se(20)	2.351(8)	Mo(4)−Se(16)	2.535(7)	Se(23)−K(4)	3.44(2)
Mo(2)−Mo(3)	2.782(8)	Se(21)−Se(22)	2.341(7)	Mo(4)−Se(19)	2.609(7)	Se(24)−K(4)	3.25(2)
Mo(4)−Mo(5)	2.759(9)	Se(23)−Se(24)	2.323(8)	Mo(4)−Se(20)	2.532(8)	Se(10)−K(5)	3.78(2)
Mo(4)−Mo(6)	2.769(8)	Se(25)−Se(26)	2.382(8)	Mo(4)−Se(21)	2.604(9)	Se(15)−K(5)	3.61(2)
Mo(5)−Mo(6)	2.760(7)	Se(4)−K(1)	3.70(2)	Mo(4)−Se(22)	2.61(1)	Se(17)−K(5)	3.39(2)
Mo(1)−Se(1)	2.495(7)	Se(4)−K(1)	3.62(2)	Mo(5)−Se(14)	2.504(8)	Se(18)−K(5)	3.77(2)
Mo(1)−Se(2)	2.629(9)	Se(12)−K(1)	3.43(2)	Mo(5)−Se(15)	2.619(9)	Se(21)−K(5)	3.37(2)
Mo(1)−Se(3)	2.54(1)	Se(13)−K(1)	3.42(2)	Mo(5)−Se(16)	2.55(1)	Se(23)−K(5)	3.28(2)
Mo(1)−Se(6)	2.591(8)	Se(21)−K(1)	3.44(2)	Mo(5)−Se(17)	2.609(8)	Se(24)−K(5)	3.31(2)
Mo(1)−Se(7)	2.535(7)	Se(25)−K(1)	3.46(2)	Mo(5)−Se(18)	2.553(9)	Se(24)−K(5)	3.73(2)
Mo(1)−Se(8)	2.586(8)	Se(26)−K(1)	3.41(2)	Mo(5)−Se(23)	2.580(8)	Se(2)−K(6)	3.61(2)
Mo(1)−Se(9)	2.633(8)	Se(4)−K(2)	3.62(2)	Mo(5)−Se(24)	2.639(7)	Se(3)−K(6)	3.79(2)
Mo(2)−Se(1)	2.51(1)	Se(5)−K(2)	3.68(2)	Mo(6)−Sc(14)	2.503(9)	Se(9)−K(6)	3.44(2)
Mo(2)−Se(2)	2.594(7)	Se(11)−K(2)	3.36(1)	Mo(6)−Se(17)	2.592(9)	Se(27)−K(6)	3.76(2)
Mo(2)−Se(3)	2.545(7)	Se(12)−K(2)	3.36(2)	Mo(6)−Se(18)	2.540(8)	K(1)−O(1)	2.71(4)
Mo(2)−Se(4)	2.609(7)	Se(19)−K(2)	3.57(1)	Mo(6)−Se(19)	2.632(9)	K(2)−O(1)	2.82(4)
Mo(2)−Se(5)	2.552(7)	Se(25)−K(2)	3.25(1)	Mo(6)−Se(20)	2.53(1)	K(2)−O(2)	2.75(3)
Mo(2)−Se(10)	2.609(9)	Se(26)−K(2)	3.55(1)	Mo(6)−Se(25)	2.619(7)	K(3)−O(3)	2.78(4)
Mo(2)−Se(11)	2.656(9)	Se(9)−K(3)	3.53(2)	Mo(6)−Se(26)	2.635(8)	K(3)−O(4)	3.11(4)
Mo(3)−Se(1)	2.486(7)	Se(13)−K(3)	3.46(2)	Se(2)−Se(3)	2.365(8)	K(3)−O(5)	3.02(5)
Mo(3)−Se(4)	2.601(9)	Se(22)−K(3)	3.23(2)	Se(4)−Se(5)	2.365(8)	K(4)−O(4)	3.31(4)
Mo(3)−Se(5)	2.542(9)	Se(26)−K(3)	3.55(2)	Se(6)−Se(7)	2.35(1)	K(5)−O(6)	2.78(5)
Mo(3)−Se(6)	2.595(9)	Se(8)−K(4)	3.54(2)	Se(8)−Se(9)	2.358(9)	K(6)−O(2)	2.61(4)
Mo(3)−Se(7)	2.533(6)	Se(10)−K(4)	3.50(2)	Se(10)−Se(11)	2.36(1)	K(6)−O(3)	2.68(4)
Mo(3)−Se(12)	2.59(1)	Se(11)−K(4)	3.43(2)	Se(12)−Se(13)	2.343(9)	K(6)−O(6)	2.75(5)
Mo(3)−Se(13)	2.622(8)	Se(14)−K(4)	3.70(2)	Se(15)−Se(16)	2.381(9)		
Mo(4)−Se(14)	2.505(9)	Se(15)−K(4)	3.60(1)				

Selected Bond Angles (deg)

Mo(2)−Mo(1)−Mo(3)	60.3(2)	Mo(5)−Mo(4)−Mo(6)	59.9(2)	Mo(1)−Mo(3)−Mo(2)	60.2(2)	Mo(4)−Mo(6)−Mo(5)	59.9(2)
Mo(2)−Mo(1)−Se(1)	56.4(3)	Mo(5)−Mo(4)−Se(14)	56.5(3)	Mo(1)−Mo(3)−Se(1)	56.5(2)	Mo(4)−Mo(6)−Se(14)	56.5(3)
Mo(2)−Mo(1)−Se(2)	57.2(2)	Mo(5)−Mo(4)−Se(15)	58.3(2)	Mo(1)−Mo(3)−Se(6)	57.8(2)	Mo(4)−Mo(6)−Se(19)	57.7(2)
Mo(2)−Mo(1)−Se(3)	56.9(2)	Mo(5)−Mo(4)−Se(16)	57.5(2)	Mo(1)−Mo(3)−Se(7)	57.0(2)	Mo(4)−Mo(6)−Se(20)	56.9(3)
Mo(3)−Mo(1)−Se(1)	56.2(2)	Mo(6)−Mo(4)−Se(14)	56.4(3)	Mo(2)−Mo(3)−Se(1)	56.5(3)	Mo(5)−Mo(6)−Se(14)	56.5(2)
Mo(3)−Mo(1)−Se(6)	57.9(2)	Mo(6)−Mo(4)−Se(19)	58.5(2)	Mo(2)−Mo(3)−Se(4)	57.8(2)	Mo(5)−Mo(6)−Se(17)	58.2(2)
Mo(3)−Mo(1)−Se(7)	57.0(2)	Mo(6)−Mo(4)−Se(20)	56.7(3)	Mo(2)−Mo(3)−Se(5)	57.1(2)	Mo(5)−Mo(6)−Se(18)	57.4(2)
Se(1)−Mo(1)−Se(2)	83.3(3)	Se(14)−Mo(4)−Se(15)	83.7(2)	Se(1)−Mo(3)−Se(4)	83.2(2)	Se(14)−Mo(6)−Se(17)	84.4(3)
Se(1)−Mo(1)−Se(3)	112.8(4)	Se(14)−Mo(4)−Se(16)	113.4(2)	Se(1)−Mo(3)−Se(5)	113.0(3)	Se(14)−Mo(6)−Se(18)	113.4(3)
Se(1)−Mo(1)−Se(6)	83.0(3)	Se(14)−Mo(4)−Se(19)	83.8(2)	Se(1)−Mo(3)−Se(6)	83.1(3)	Se(14)−Mo(6)−Se(19)	83.4(3)
Se(1)−Mo(1)−Se(7)	112.5(2)	Se(14)−Mo(4)−Se(20)	112.5(2)	Se(1)−Mo(3)−Se(7)	112.9(2)	Se(14)−Mo(6)−Se(20)	112.8(3)
Se(1)−Mo(1)−Se(8)	92.3(3)	Se(14)−Mo(4)−Se(21)	96.4(3)	Se(1)−Mo(3)−Se(12)	93.1(3)	Se(14)−Mo(6)−Se(25)	94.4(2)
Se(1)−Mo(1)−Se(9)	145.8(3)	Se(14)−Mo(4)−Se(22)	149.7(3)	Se(1)−Mo(3)−Se(13)	146.4(3)	Se(14)−Mo(6)−Se(26)	147.9(3)
Se(2)−Mo(1)−Se(3)	54.4(2)	Se(15)−Mo(4)−Se(16)	55.1(2)	Se(4)−Mo(3)−Se(5)	54.7(2)	Se(17)−Mo(6)−Se(18)	54.3(2)
Se(2)−Mo(1)−Se(6)	165.4(2)	Se(15)−Mo(4)−Se(19)	166.4(2)	Se(4)−Mo(3)−Se(6)	165.3(2)	Se(17)−Mo(6)−Se(19)	167.2(2)
Se(2)−Mo(1)−Se(7)	136.4(3)	Se(15)−Mo(4)−Se(20)	136.7(2)	Se(4)−Mo(3)−Se(7)	137.0(3)	Se(17)−Mo(6)−Se(20)	135.6(3)
Se(2)−Mo(1)−Se(8)	86.6(2)	Se(15)−Mo(4)−Se(21)	88.3(2)	Se(4)−Mo(3)−Se(12)	87.5(2)	Se(17)−Mo(6)−Se(25)	86.1(3)
Se(2)−Mo(1)−Se(9)	96.8(3)	Se(15)−Mo(4)−Se(22)	94.5(2)	Se(4)−Mo(3)−Se(13)	96.3(3)	Se(17)−Mo(6)−Se(26)	96.7(2)
Se(3)−Mo(1)−Se(6)	136.7(3)	Se(16)−Mo(4)−Se(19)	136.1(3)	Se(5)−Mo(3)−Se(6)	136.9(2)	Se(18)−Mo(6)−Se(19)	135.5(2)
Se(3)−Mo(1)−Se(7)	82.4(3)	Se(16)−Mo(4)−Se(20)	81.9(2)	Se(5)−Mo(3)−Se(7)	82.6(4)	Se(18)−Mo(6)−Se(20)	81.6(2)
Se(3)−Mo(1)−Se(8)	127.8(3)	Se(16)−Mo(4)−Se(21)	127.0(3)	Se(5)−Mo(3)−Se(12)	128.2(3)	Se(18)−Mo(6)−Se(25)	126.1(3)
Se(3)−Mo(1)−Se(9)	94.0(3)	Se(16)−Mo(4)−Se(22)	89.3(2)	Se(5)−Mo(3)−Se(13)	93.2(2)	Se(18)−Mo(6)−Se(26)	92.3(3)
Se(6)−Mo(1)−Se(7)	54.7(3)	Se(19)−Mo(4)−Se(20)	54.4(2)	Se(6)−Mo(3)−Se(7)	54.6(3)	Se(19)−Mo(6)−Se(20)	54.2(3)
Se(6)−Mo(1)−Se(8)	89.1(3)	Se(19)−Mo(4)−Se(21)	87.6(2)	Se(6)−Mo(3)−Se(12)	88.0(3)	Se(19)−Mo(6)−Se(25)	90.7(3)
Se(6)−Mo(1)−Se(9)	91.8(3)	Se(19)−Mo(4)−Se(22)	93.5(2)	Se(6)−Mo(3)−Se(13)	92.2(3)	Se(19)−Mo(6)−Se(26)	91.5(2)
Se(7)−Mo(1)−Se(8)	130.3(3)	Se(20)−Mo(4)−Se(21)	126.7(3)	Se(7)−Mo(3)−Se(12)	128.6(3)	Se(20)−Mo(6)−Se(25)	129.8(2)
Se(7)−Mo(1)−Se(9)	90.9(2)	Se(20)−Mo(4)−Se(22)	89.5(3)	Se(7)−Mo(3)−Se(13)	90.4(2)	Se(20)−Mo(6)−Se(26)	88.7(2)
Se(8)−Mo(1)−Se(9)	53.7(2)	Se(21)−Mo(4)−Se(22)	53.3(2)	Se(12)−Mo(3)−Se(13)	53.4(2)	Se(25)−Mo(6)−Se(26)	53.9(2)
Mo(1)−Mo(2)−Mo(3)	59.5(2)	Mo(4)−Mo(5)−Mo(6)	60.2(2)	Mo(1)−Se(1)−Mo(2)	67.6(3)	Mo(4)−Se(14)−Mo(5)	66.9(2)
Mo(1)−Mo(2)−Se(1)	56.0(2)	Mo(4)−Mo(5)−Se(14)	56.6(2)	Mo(1)−Se(1)−Mo(3)	67.3(2)	Mo(4)−Se(14)−Mo(6)	67.1(2)
Mo(1)−Mo(2)−Se(2)	58.4(2)	Mo(4)−Mo(5)−Se(15)	57.9(2)	Mo(2)−Se(1)−Mo(3)	67.7(2)	Mo(5)−Se(14)−Mo(6)	66.9(2)
Mo(1)−Mo(2)−Se(3)	56.8(3)	Mo(4)−Mo(5)−Se(16)	56.9(3)	Mo(1)−Se(2)−Mo(2)	64.4(2)	Mo(4)−Se(15)−Mo(5)	63.7(2)
Mo(3)−Mo(2)−Se(1)	55.8(2)	Mo(6)−Mo(5)−Se(14)	56.5(2)	Mo(1)−Se(2)−Se(3)	60.9(3)	Mo(4)−Se(15)−Se(16)	60.9(2)
Mo(3)−Mo(2)−Se(4)	57.6(2)	Mo(6)−Mo(5)−Se(17)	57.7(2)	Mo(2)−Se(2)−Se(3)	61.6(2)	Mo(5)−Se(15)−Se(16)	61.2(3)
Mo(3)−Mo(2)−Se(5)	56.7(2)	Mo(6)−Mo(5)−Se(18)	57.0(2)	Mo(1)−Se(3)−Mo(2)	66.3(3)	Mo(4)−Se(16)−Mo(5)	65.7(2)
Se(1)−Mo(2)−Se(2)	83.8(2)	Se(14)−Mo(5)−Se(15)	83.5(3)	Mo(1)−Se(3)−Se(2)	64.7(3)	Mo(4)−Se(16)−Se(15)	64.0(2)
Se(1)−Mo(2)−Se(3)	112.3(4)	Se(14)−Mo(5)−Se(16)	112.9(3)	Mo(2)−Se(3)−Se(2)	63.6(2)	Mo(5)−Se(16)−Se(15)	64.0(2)
Se(1)−Mo(2)−Se(4)	82.6(2)	Se(14)−Mo(5)−Se(17)	84.1(3)	Mo(2)−Se(4)−Mo(3)	64.6(2)	Mo(5)−Se(17)−Mo(6)	64.1(2)
Se(1)−Mo(2)−Se(5)	111.9(3)	Se(14)−Mo(5)−Se(18)	112.9(3)	Mo(2)−Se(4)−Se(5)	61.5(2)	Mo(5)−Se(17)−Se(18)	61.8(3)
Se(1)−Mo(2)−Se(10)	93.4(3)	Se(14)−Mo(5)−Se(23)	92.8(2)	Mo(3)−Se(4)−Se(5)	61.4(3)	Mo(6)−Se(17)−Se(18)	61.7(3)
Se(1)−Mo(2)−Se(11)	146.7(2)	Se(14)−Mo(5)−Se(24)	145.4(2)	Mo(2)−Se(5)−Mo(3)	66.2(2)	Mo(5)−Se(18)−Mo(6)	65.6(2)
Se(2)−Mo(2)−Se(3)	54.8(2)	Se(15)−Mo(5)−Se(16)	54.8(3)	Mo(2)−Se(5)−Se(4)	64.0(2)	Mo(5)−Se(18)−Se(17)	64.3(2)
Se(2)−Mo(2)−Se(4)	165.5(2)	Se(15)−Mo(5)−Se(17)	166.9(3)	Mo(3)−Se(5)−Se(4)	63.9(3)	Mo(6)−Se(18)−Se(17)	64.0(3)
Se(2)−Mo(2)−Se(5)	136.6(2)	Se(15)−Mo(5)−Se(18)	136.1(3)	Mo(1)−Se(6)−Mo(3)	64.3(2)	Mo(4)−Se(19)−Mo(6)	63.8(2)
Se(2)−Mo(2)−Se(10)	88.3(2)	Se(15)−Mo(5)−Se(23)	90.5(3)	Mo(1)−Se(6)−Se(7)	61.4(2)	Mo(4)−Se(19)−Se(20)	61.1(2)
Se(2)−Mo(2)−Se(11)	93.9(2)	Se(15)−Mo(5)−Se(24)	92.1(2)	Mo(3)−Se(6)−Se(7)	61.3(2)	Mo(6)−Se(19)−Se(20)	60.6(3)
Se(3)−Mo(2)−Se(4)	136.2(2)	Se(16)−Mo(5)−Se(17)	135.2(3)	Mo(1)−Se(7)−Mo(3)	66.0(2)	Mo(4)−Se(20)−Mo(6)	66.4(2)
Se(3)−Mo(2)−Se(5)	82.1(2)	Se(16)−Mo(5)−Se(18)	81.6(2)	Mo(1)−Se(7)−Se(6)	63.9(2)	Mo(4)−Se(20)−Se(19)	64.5(2)
Se(3)−Mo(2)−Se(10)	129.8(3)	Se(16)−Mo(5)−Se(23)	131.3(3)	Mo(3)−Se(7)−Se(6)	64.0(3)	Mo(6)−Se(20)−Se(19)	65.2(2)
Se(3)−Mo(2)−Se(11)	92.6(4)	Se(16)−Mo(5)−Se(24)	91.5(3)	Mo(1)−Se(8)−Se(9)	64.2(3)	Mo(4)−Se(21)−Se(22)	63.5(4)
Se(4)−Mo(2)−Se(5)	54.5(2)	Se(17)−Mo(5)−Se(18)	53.9(2)	Mo(1)−Se(9)−Se(8)	62.1(2)	Mo(4)−Se(22)−Se(21)	63.2(3)
Se(4)−Mo(2)−Se(10)	87.5(2)	Se(17)−Mo(5)−Se(23)	85.8(3)	Mo(2)−Se(10)−Se(11)	64.3(2)	Mo(5)−Se(23)−Se(24)	64.9(2)
Se(4)−Mo(2)−Se(11)	94.7(3)	Se(17)−Mo(5)−Se(24)	95.7(3)	Mo(2)−Se(11)−Se(10)	62.3(3)	Mo(5)−Se(24)−Se(23)	62.3(2)
Se(5)−Mo(2)−Se(10)	128.5(2)	Se(18)−Mo(5)−Se(23)	126.7(3)	Mo(3)−Se(12)−Se(13)	63.9(3)	Mo(6)−Se(25)−Se(26)	63.4(2)
Se(5)−Mo(2)−Se(11)	92.5(3)	Se(18)−Mo(5)−Se(24)	93.9(3)	Mo(3)−Se(13)−Se(12)	62.7(3)	Mo(6)−Se(26)−Se(25)	62.7(3)
Se(10)−Mo(2)−Se(11)	53.4(3)	Se(23)−Mo(5)−Se(24)	52.9(2)				

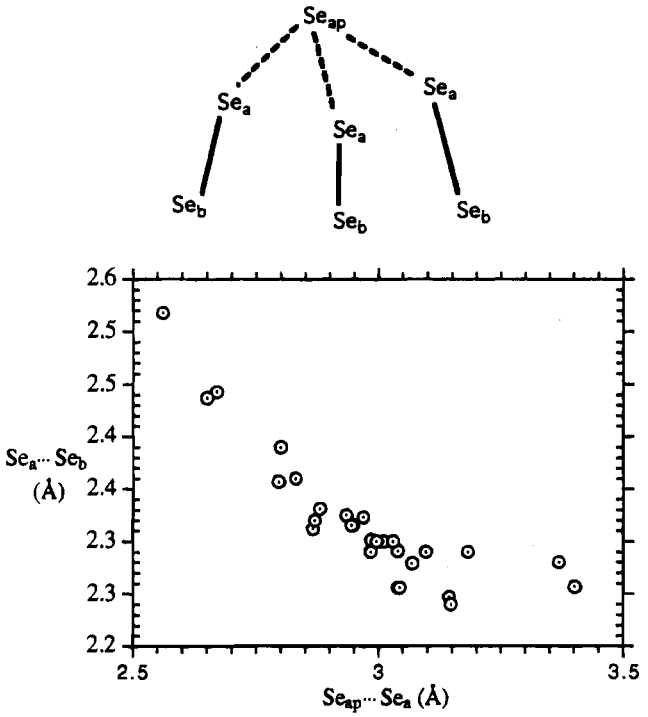

Figure 7. Se−Se bond correlation. The horizontal axis represents the Se_{ap}−Se_a bond variation in different Mo selenide molecules. The corresponding Se_a−Se_b is plotted as a function of the Se_{ap}−Se_a distance.

plane, and OP(∞), the corresponding overlap population as d approaches infinity. A shift to positive Δ(O) values indicates a strengthening of the corresponding interatomic bond. It is clear from these plots that our prediction is consistent with the experimental findings: strong bonding interactions are observed between Se_a (labeled Se(8), Se(9), and Se(10)) and $Se(17)^{2-}$ when the latter is brought close to the $[Mo_3Se_{13}]^{2-}$ trinuclear cluster. At d = 3.6 Å, which corresponds to an interatomic distance of Se(8)−Se(17) = 2.60 Å and Se(9)−Se(17) = 2.81 Å, the overlap populations for the two bonds are increased from zero to 0.106 and 0.018 respectively. At the same time, the decrease in the overlap population between Se_a and Se_b, that is Se(5)−Se(8) (or Se(7)−Se(10), equivalent by symmetry) and Se(6)−Se(9), indicates a significant bond weakening between the two atoms. For example, at d = 3.6 Å, Δ(O) is −0.163 for Se(5)−Se(8) and is −0.072 for Se(6)−Se(9). Notice the strong correlation between the Se_{ap}−Se_a and Se_a−Se_b pairs: at a given d, the stronger the bond between Se_{ap} and Se_a, the bigger the decrease in the Se_a−Se_b bond strength. This is in complete agreement with the experimental data and suggests a significant electron transfer from the Se_{ap}^{2-} to the trinuclear cluster and particularly to the antibonding orbitals of the Se_a−Se_b bridging unit.

It is also interesting to observe the overlap population increase in the Mo−Mo bonds and the repulsive interactions between these metals and the Se^{2-} atom. At d = 3.6 Å, or equivalently at Se(8)−Se(17) = 2.6 Å and Se(9)−Se(17) = 2.81 Å, the increase in the overlap population is calculated to be 0.019 and 0.026 for the Mo(1)−Mo(2) and Mo(1)−Mo(3) bonds respectively. This unexpected metal-metal bond strengthening appeared to be most pronounced in $K_{12}Mo_{12}Se_{56}$ which has the strongest $[Mo_3Se_7]^{4+}\cdots Se_{ap}$ interactions. In this compound the average Mo−Mo distances of 2.75(2) Å are the shortest among the clusters while those in $(Me_4N)_2Mo_3Se_{13}$ and $K_2Mo_3Se_{12.5}O_{0.5}$ are slightly longer at 2.784(6) and 2.771(1) Å respectively. For the same d, the decreases in the Mo(1)−Se(17) and Mo(3)−Se(17) overlap populations are up to 0.051 and 0.073 suggesting repulsive interactions. Other bonds, mainly the Mo−(μ_3-Se),

Table 8. Relationship of Se···Se Contacts between Se^{2-} and $[Mo_3Se_7]^{4+}$ Core and Their Corresponding Bridging Se_2^{2-} and Mo−se Bond Lengths[a]

compound	*a*1	*a*2	*a*3	*x*1	*x*2	*x*3	*m*1	*m*2
$(Me_4N)_2Mo_3Se_{13}$	3.147(7)	3.147(7)	3.147(7)	2.290(6)	2.290(6)	2.290(6)	2.784(6)	2.784(6)
$K_2Mo_3Se_{13}$	3.044(9)	3.029(6)	3.029(6)	2.306(6)	2.303(4)	2.303(4)	2.772(3)	2.771(2)
α-$K_8Mo_9Se_{40}$·$4H_2O$	2.886(9)	2.969(7)	2.80(1)	2.362(8)	2.373(8)	2.44(1)	2.791(5)	2.772(6)
	2.984(8)	3.182(9)	2.87(1)	2.340(8)	2.349(9)	2.37(1)	2.773(6)	2.750(6)
	3.14(1)	3.04(1)	3.19(1)	2.297(8)	2.329(7)	2.307(8)	2.760(6)	2.749(6)
$K_2Mo_3Se_{18}$	3.33793)	3.097(3)	2.996(3)	2.330(3)	2.340(3)	2.350(3)	2.779(2)	2.781(2)
$K_{12}Mo_{12}Se_{56}$	2.561(9)	2.796(9)	2.934(9)	2.568(9)	2.407(9)	2.375(9)	2.756(7)	2.758(7)
	2.67(1)	2.67(1)	2.83(1)	2.493(9)	2.493(9)	2.41(1)	2.735(8)	2.735(8)
	3.03(1)	2.65(1)	2.65(1)	2.35(1)	2.487(9)	2.487(9)	2.73(1)	2.733(8)
$K_6Mo_6Se_{27}$·$6H_2O$	2.945(8)	2.947(8)	3.01(1)	2.365(8)	2.365(8)	2.35(1)	2.782(8)	2.781(9)
	2.88(1)	3.04(1)	2.985(8)	2.381(9)	2.341(8)	2.351(8)	2.759(9)	2.760(7)

[a] Uniform labeling scheme for the interaction of Se^{2-} with a $[Mo_3Se_{13}]^{2-}$ cluster.

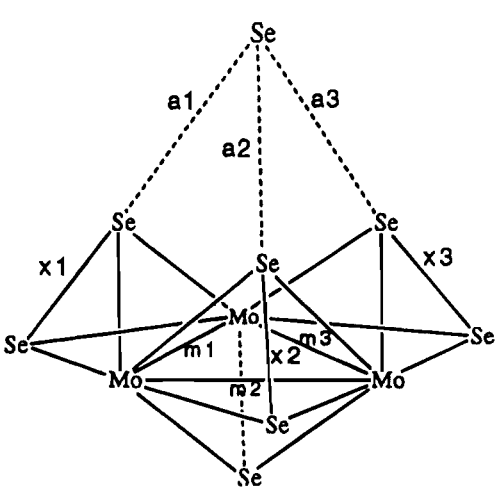

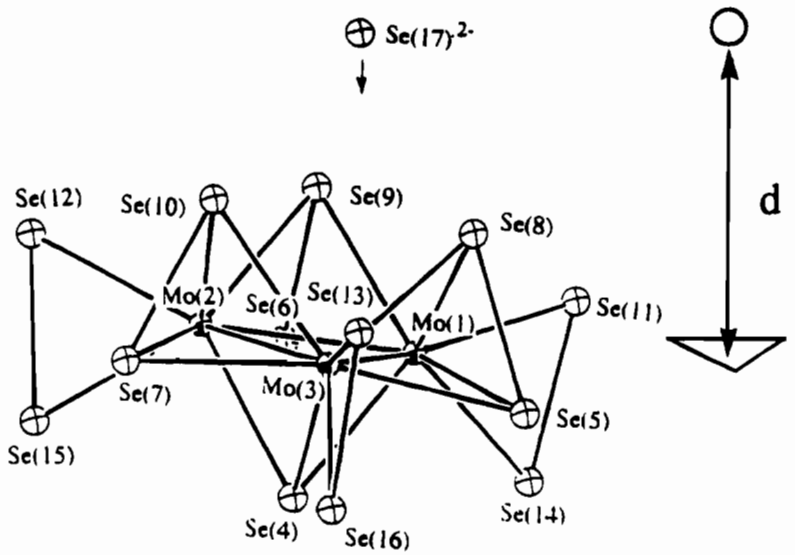

Figure 8. Se^{2-} approaching the $[Mo_3Se_{13}]^{2-}$ cluster. The labeling scheme used for the MO calculation is shown.[23]

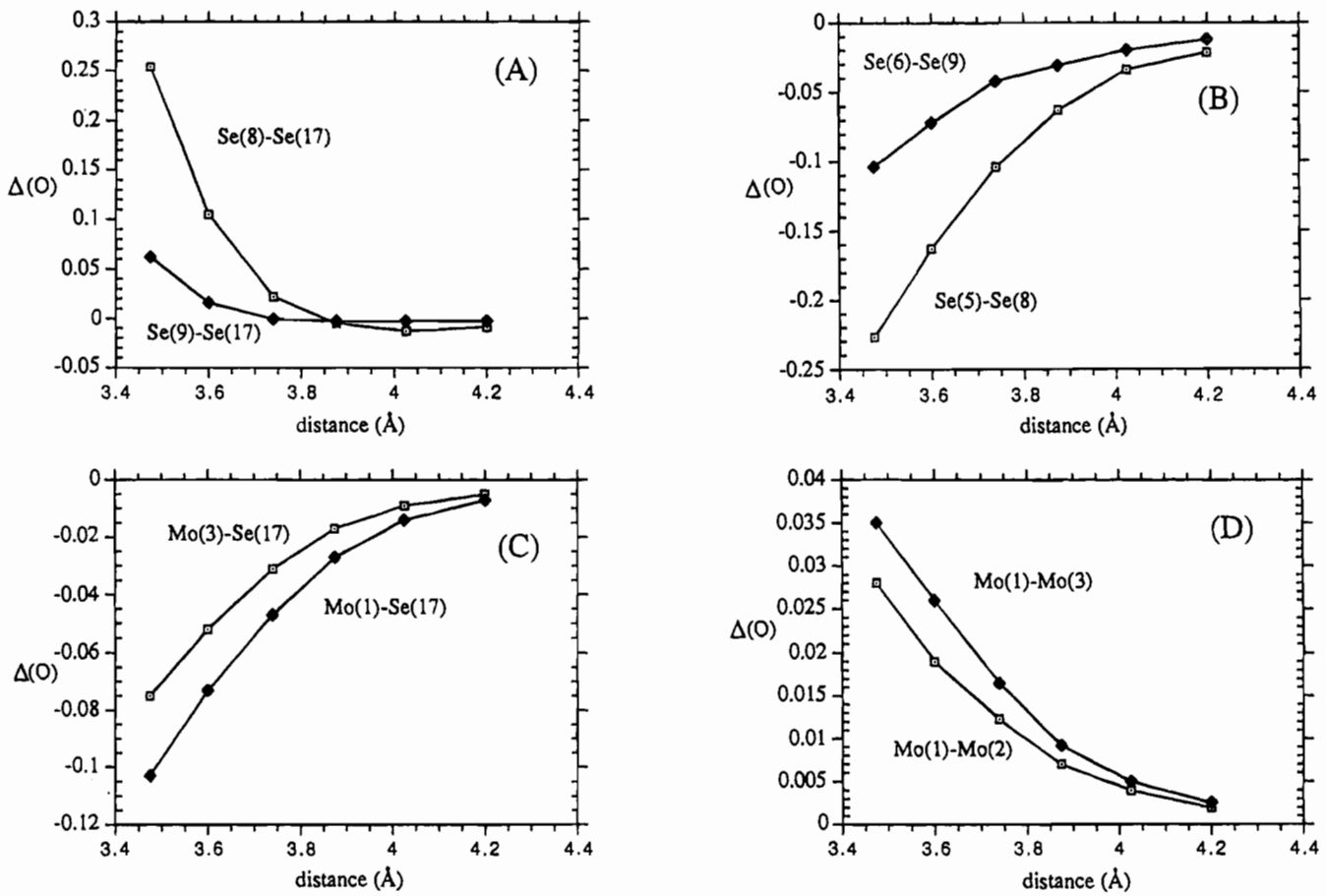

Figure 9. Changes in the overlap population, Δ(O), as a function of d, the distance between the Se^{2-} anion and the Mo_3 plane: (A) $Mo-Se^{2-}$ bonds, (B) Se_a-Se_b bonds, (C) $Se^{2-}-Se_a$ bonds, and (D) the Mo−Mo bonds. The Se^{2-} is labeled as Se(17), Se_a as Se(8), Se(9) and Se_b as Se(5), Se(6). Atoms Se(7) and Se(10) are equivalent to Se(5) and Se(8) respectively and they are not shown in the figure.

$Mo-Se_a$, $Mo-Se_b$, $Mo-Se_2$(terminal), and terminal Se−Se bonds, remain almost unaffected.

The calculated electron distribution in $[Mo_3Se_{13}]^{2-}$ helps in understanding why an incoming negatively charged Se_{ap} atom tends to form bonds with the also negatively charged trinuclear cluster and why it approaches preferably the doubly bridged Se_2^{2-} rather than other Se atoms in the cluster. Of the five types of selenium atoms present in a $[Mo_3Se_{13}]^{2-}$ cluster the terminal diselenides are the most negatively charged. While μ_3-Se carries a smaller negative charge, the doubly bridging Se_a atoms are the most electron poor with a calculated 0.185 electron loss. Therefore Se_a becomes the most suitable site for anionic attack by a Se_{ap} atom such as Se^{2-}. The presence of a positive charge on a μ-Se_2^{2-} unit is difficult to anticipate with classical intuitive arguments and underscores the usefulness of the MO calculation. Changes in the electron density of individual atoms in the $\{[Mo_3Se_{13}]^{2-}\cdot Se^{2-}\}$ model system, as a function of the $Mo\cdots Se_{ap}^{2-}$ distance are given in Figure 10, which clearly shows that charge transfer occurs as the Se_{ap}^{2-} atom approaches the trinuclear cluster. Se_{ap}^{2-} appears to suffer the greatest electron loss of 0.96, going from $d = \infty$ to $d = 3.6$ Å. This electron density ends up largely on the metal atoms

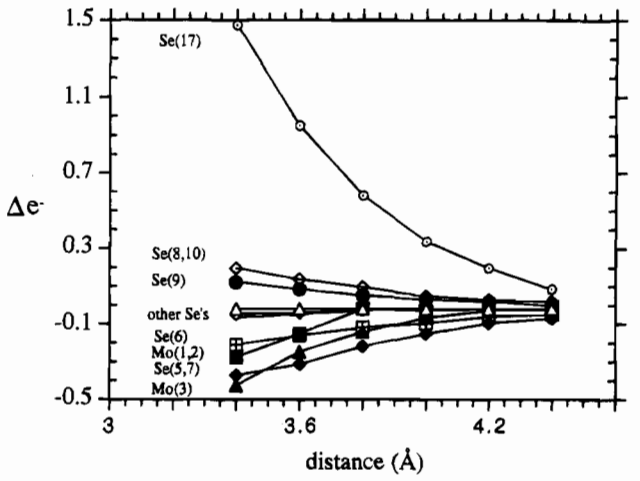

Figure 10. Electron density change for all atoms. Δe^- is the difference between the electron density of an atom in $\{[Mo_3Se_{13}]^{2-}\cdot Se^{2-}\}$ at various distances, d, and in the extreme case where d = ∞.

and the Se_b atoms, as indicated in the plot. At d = 3.6 Å, a total gain of 0.145 electrons for each Mo atom, and 0.284 electrons for Se(5) and Se(7) are calculated. The Se_a atoms, previously positively charged, have a further loss of 0.150 electrons for Se(8) and Se(10), and 0.083 electron for Se(9).

In the above discussion we have showed what happens when an additional ligand, Se_{ap}, interacts with the trinuclear cluster $[Mo_3Se_{13}]^{2-}$. To understand the bonding nature of such interactions it is useful to take a closer look at the orbital interaction diagram sketched in Figure 11. Outlined in the three boxes are the important frontier molecular orbitals for d = 3.4 (left), 3.8 (middle) and 4.2 Å (right) respectively. The orbital energies of the two fragments $[Mo_3Se_{13}]^{2-}$ and Se^{2-} are drawn on either side of each box. The highest occupied molecular orbitals (HOMO) are nos. 31 and 32 in all three cases. At large distance between the two fragments, for example d = 3.8 and 4.2 Å as in (b) and (c), these orbitals mostly consist of the metal 4d orbitals. For smaller d as in (a), however, these metal centered orbitals become nos. 33 and 34. Several occupied frontier orbitals, for example, the MO 31a″ and 32a′ in (a), or equivalently the MO 33a′/34a″ in (b), and MO 37a′/38a″ in (c), contain largely contributions from a number of high-lying unoccupied $[Mo_3Se_{13}]^{2-}$ orbitals, such as nos. 19, 22−24, and 27. Orbital overlap population analysis shows that, in general, these orbitals are *bonding* between the metal atoms (Mo−Mo) and antibonding between the doubly bridging Se_2^{2-} atoms (Se_a and Se_b), and on average, is greater in magnitude for the latter. For example, the fragment molecular orbitals (FMO) nos. 19 and 24 of $[Mo_3Se_{13}]^{2-}$ contribute an overlap population of 0.022 and 0.031, respectively, to both Mo(1)−Mo(2) and Mo(1)−Mo(3) bonds and −0.043 and −0.061, respectively, to both Se(5)−Se(8) and Se(6)−Se(9) bonds when occupied by two electrons. Upon formation of the $\{[Mo_3Se_{13}]^{2-}\cdot Se^{2-}\}$ aggregate, these orbitals interact with the Se_{ap}^{2-} orbitals in a bonding fashion. When the two fragments interact strongly as in (a), the orbital overlaps are the greatest which lead to a large contribution of these orbitals to the MO 31a″ and 32a′ that are fully occupied. The FMO nos. 24 and 27, for instance, contribute a total of 30% to MOs 32a″ and 31a′ respectively. A pictorial representation of these orbital interactions in the two HOMO's is shown in Figure 12. The antibonding nature of the interaction between the two Se atoms (Se_a and Se_b) is clearly demonstrated in the figure. As the two fragments are pulled apart as in (b) and (c), the orbital overlaps are significantly

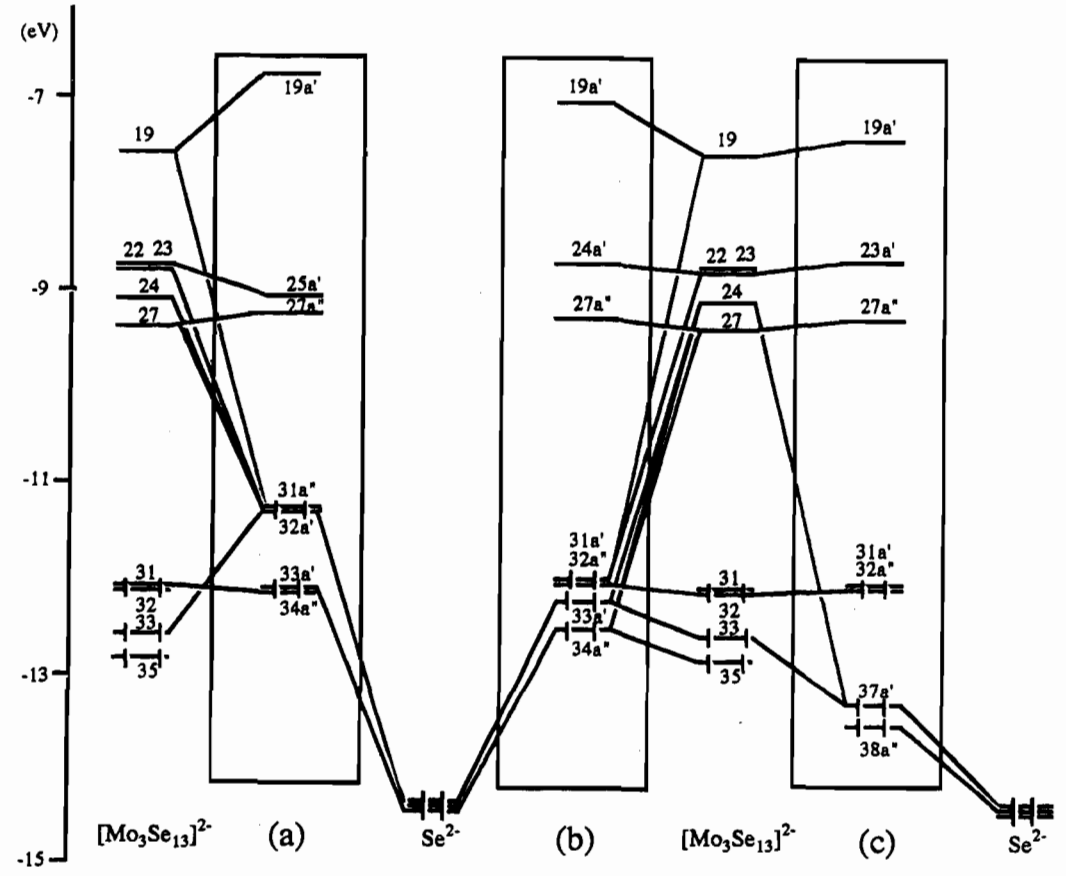

Figure 11. Orbital interaction diagram for the $\{[Mo_3Se_{13}]^{2-}\cdot Se^{2-}\}$ model system. Three situations are considered: (a) d = 3.4 Å, (b) d = 3.8 Å, and (c) d = 4.2 Å. The molecular orbital levels of interest are sketeched in the central area in each case and are outlined within a box; a′ and a″ are the symmetry labels for these orbitals. The corresponding fragment orbital energies of $[Mo_3Se_{13}]^{2-}$ and Se^{2-} are drawn on either side of each box. MO Nos. 33 and 34 are mainly Mo_3 4d orbital combinations (33, 83%; 34, 100%).

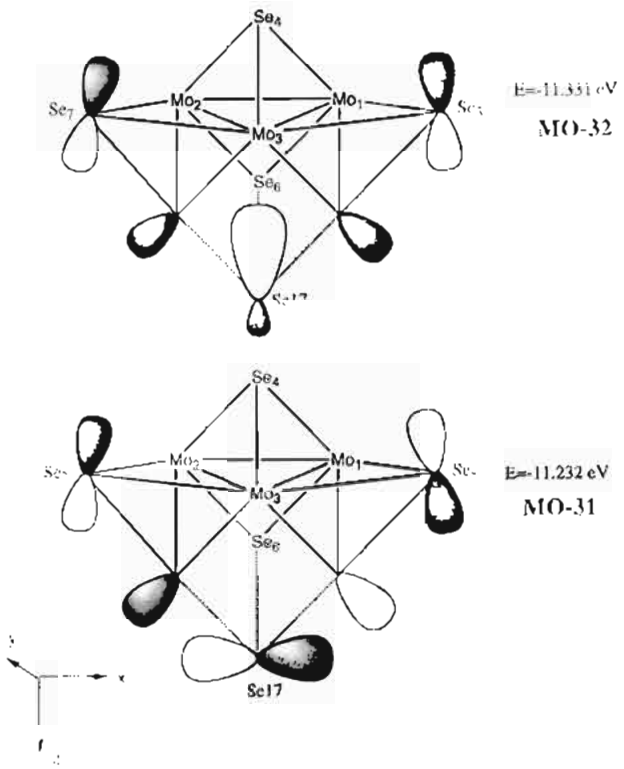

Figure 12. Plots of two $\{[Mo_3Se_{13}]^{2-}\cdot Se^{2-}\}$ aggregate HOMO's, Nos. 31 and 32, in case (a) [defined in Figure 11] are shown. As described in the text, MO nos. 31 and 32 contain mainly contributions from the high-lying unoccupied Se_a-Se_b antibonding orbitals [e.g. nos. 23–24, 27 of the fragment $(Mo_3Se_{13})^{2-}$] and the Se_{ap}^{2-} orbitals. For clarity, the terminal Se_2^{2-} units are not shown. Also small contributions to these MOs from Mo d-orbitals have been omitted. The antibonding nature between Se_a and Se_b is clearly visible. As the apical Se^{2-} is removed from the $[Mo_3Se_{13}]^{2-}$ cluster, i.e. in cases (b) and (c), these orbitals continue to look similar but with much greater contributions from Se_{ap}^{2-} and much less from the bridging Se_2^{2-}. In these two cases the electron transfer to the Se_a-Se_b antibonding orbitals is considerably retarded. In other words, the HOMO's shown above possess less Se_a-Se_b antibonding character.

reduced. Consequently, the interactions between the two fragments are much weakened and these vacant high-lying $[Mo_3Se_{13}]^{2-}$ fragment orbitals contribute much less to the corresponding molecular orbitals (33a′ and 34a″ in (b), 37a′ and 38a″ in (c)). In fact, the fragment orbitals nos. 19, 22–23, and 27 of $[Mo_3Se_{13}]^{2-}$ give essentially no contributions to the molecular orbital 37a′ and 38a″ in case (c). These FMO contributions are plotted in Figure 13 as a function of the distance. Notice that the metal-centered molecular orbitals, that is 33a′ and 34a″ in (a) and 31a′ and 32a″ in both (b) and (c) are essentially the same at all distances.

The conclusion that we may draw from the above analysis is that the extent of the interactions between the two fragments, Se^{2-} and $[Mo_3Se_{13}]^{2-}$, determines the amount of the Se_a-Se_b antibonding character in the highest occupied molecular orbitals (Se centered). The stronger the interactions between the two,

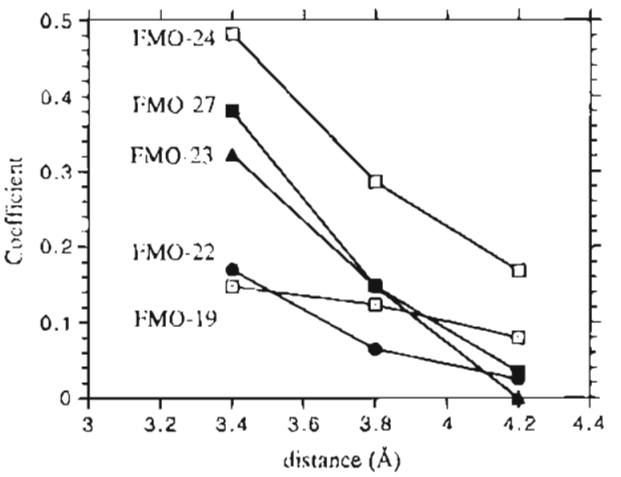

Figure 13. Contributions of the fragment molecular orbitals (FMO) of $[Mo_3Se_{13}]^{2-}$ to the molecular orbitals (MO) 31a′, 32a″ (d = 3.4 Å), 33a′, 34a″ (d = 3.8 Å) and 37a′, 38a″ (d = 4.2 Å). C is the coefficient of the FMO in the MO.

the more the Se_a-Se_b bonds are weakened. Correspondingly a less pronounced and opposite effect applies to the Mo–Mo bonds.

Concluding Remarks

Thus far, all hydrothermally synthesized Mo/Se phases contain $[Mo_3(\mu_2\text{-}Se_2)_3Se]^{4+}$ cluster cores bound by polyselenide ligands. This extraordinarily stable trinuclear core contains a triangular cavity created by the selenium atoms of the $\mu_2\text{-}Se_2^{2-}$ ligands and posseses the unusual property of attracting electron-rich species such as Se^{2-} or Se_x^{2-} ligands. Extended Hückel MO calculations suggest that the "pancake-like" $[Mo_3Se_{13}]^{2-}$ cluster has an uneven electron distribution so that one side, containing the triangular selenium cavity, is positively charged while the opposite side (containing the $\mu_3\text{-}Se^{2-}$ anion) is negatively charged. Thus, the so-called anion–anion interactions are in fact coulombically driven attractions between electron-rich anions and the electron-poor side of the trinuclear $[Mo_3Se_{13}]^{2-}$ cluster. These interactions should be general in nature and should lead to new adduct complexes of the type $\{[Mo_3Se_{13}]^{2-}\cdot X\}$, where X is an electron-rich species.[21]

Acknowledgment. We thank the National Science Foundation for a Presidential Young Investigator Award (1989–1994) and the donors of the Petroleum Research Fund, administered by the American Chemical Society, for financial support of this research. M.G.K. is a Camille and Henry Dreyfus Teacher-Scholar 1993–1995.

Supplementary Material Available: Tables of calculated and observed X-ray powder diffraction patterns, positional and anisotropic thermal parameters of all atoms, a complete table of crystallographic data for $(Me_4N)_2Mo_3Se_{13}$, $K_2Mo_3Se_{12.5}O_{0.5}$ and $K_6Mo_6Se_{27}\cdot 6H_2O$, and computer-drawn figures showing FMO nos. 31 and 32. (12 pages). Ordering information is given on any current masthead page.

IC941122T